Chemical Engineering Journal 524 (2025) 168431

Contents lists available at ScienceDirect

Chemical Engineering Journal

journal homepage: www.elsevier.com/locate/cej

Biological upcycling of polystyrene into ready-to-use plastic monomers and plastics using metabolically engineered *Pseudomonas putida*

Michael Kohlstedt [a], Fabia Weiland [a], Samuel Pearson [b], Devid Hero [c], Sophia Mihalyi [d], Laurenz Kramps [e], Georg Gübitz [d], Markus Gallei [c,f], Aránzazu del Campo [b], Christoph Wittmann [a,*]

[a] Institute of Systems Biotechnology, Saarland University, Saarbrücken, Germany
[b] Dynamic Biomaterials Group, Leibniz Institute for New Materials (INM), Saarbrücken, Germany
[c] Institute of Polymer Chemistry, Saarland University, Saarbrücken, Germany
[d] Institute of Environmental Biotechnology, University of Natural Resources and Life Sciences, Vienna, Austria
[e] Taros Chemicals GmbH, Dortmund, Germany
[f] Saarene, Saarland Center for Energy Materials and Sustainability, Saarbrücken, Germany

ARTICLE INFO

Keywords:
Polystyrene upcycling
Pseudomonas putida
Muconic acid
Adipic acid
Hexamethylenediamine
Nylon

ABSTRACT

The persistent accumulation of plastic waste, particularly polystyrene (PS), poses significant environmental challenges because of its extensive use and low recycling rates. Addressing these challenges necessitates innovative and sustainable solutions. This study presents a strategy to upcycle PS waste into valuable chemical products, including adipic acid, hexanediol, hexamethylenediamine, and nylon-6,6, using metabolically engineered *Pseudomonas putida* KT2440. This process involves the photolytic degradation of PS into benzoic acid, followed by microbial conversion into *cis,cis*-muconate (MA) and chemical synthesis of the final products. The engineered strains withstood 30 mM concentrations of PS-derived aromatics and converted them stoichiometrically into MA in the presence of glucose as a growth substrate. ^{13}C metabolic flux analysis revealed energy and redox limitations in the presence of 25 mM benzoate and 300 mM MA. The cells responded to stress by enhancing the flux for periplasmic glucose oxidation and fluxes through the NADPH-forming dehydrogenases; this process caused more than 40 % glucose-carbon loss into byproducts. Fine-tuned dynamic glucose and benzoate feeding enabled high-level MA production. Energy-optimized genome-reduced strains were used to increase carbon efficiency. A final MA titer of over 65 g L^{-1} was achieved in fed-batch fermentation. This process was demonstrated using the glucose derived from a viscose textile waste blend as the growth substrate and resulted in fully waste-based products. The resulting adipic acid and hexamethylenediamine were polymerized into nylon-6,6 with properties comparable to those of petrochemical-derived polymers, revealing a sustainable pathway for PS upcycling. This research provides a proof-of-concept for bacterial upgrading of PS-derived substrates and a viable method for managing plastic waste and producing valuable chemical products.

1. Introduction

Plastic accumulation poses a persistent global challenge [1]. Polystyrene (PS), widely used in packaging and single-use goods, is a major contributor to plastic waste and microplastic pollution [2]. Despite >20 Mt. annual PS production [3], recycling remains <10 % due to economic and technical barriers [4]. Prior efforts have focused on depolymerizing PS to aromatic monomers for recovery and reuse [5–10], but end-to-end routes that convert PS into drop-in polymer precursors and validate final polymer performance remain scarce.

This work introduces a fully integrated, waste-based value chain from PS to nylon-6,6, combining (i) photolytic depolymerization of PS to benzoate using mild conditions, (ii) microbial upgrading by metabolically engineered *Pseudomonas putida* to produce *cis,cis*-muconic acid (MA), and (iii) chemical transformations of MA to adipic acid, hexanediol, and hexamethylenediamine, culminating in nylon-6,6 with petrochemical-equivalent properties. The process further leverages textile-derived glucose as a growth substrate, enabling a dual-waste,

* Corresponding author.
E-mail address: christoph.wittmann@uni-saarland.de (C. Wittmann).

https://doi.org/10.1016/j.cej.2025.168431
Received 25 March 2025; Received in revised form 4 September 2025; Accepted 12 September 2025
Available online 15 September 2025

fully waste-based concept. At the bioprocess core, we deploy a precision fermentation strategy guided by ^{13}C metabolic flux analysis, using dynamic glucose dosing and DO-coupled benzoate feeding to sustain productivity under substrate/product stress. We also evaluate a genome-reduced chassis for improved carbon efficiency and robustness.

P. putida is a versatile host with broad aromatic catabolism and industrial robustness [11–16]. Through pathway engineering, it efficiently channels aromatics to MA, a valuable platform chemical [17–21], and synthetic biology has broadened its repertoire to additional products [22–25]. What distinguishes this study is the system-level integration: we (i) convert PS directly to a fermentable intermediate (benzoate), (ii) demonstrate high-efficiency microbial upgrading of both commercial and crude PS-derived benzoate, (iii) replace virgin sugar with textile-derived glucose, and (iv) close the loop to nylon-6,6, confirming material parity. The combined flux-guided control and waste-only feedstocks address key roadblocks in PS valorization—namely, inhibitory aromatic stress, by-product formation, and dependency on virgin substrates.

In summary, this study delivers a novel, end-to-end, fully waste-based route from PS to adipic acid, 1,6-hexanediol, hexane-1,6-diamine, and nylon-6,6 by integrating gentle photochemical depolymerization, engineered microbial conversion, and industrial-relevant downstream chemistry, underpinned by quantitative flux analysis and dynamic process control. This framework advances PS upcycling beyond monomer recovery toward specification-grade polymer precursors and materials, offering a practical pathway for circular manufacturing.

2. Materials and methods

2.1. Strains and plasmids

P. putida KT2440 and its MA-producing derivatives *P. putida* MA-1 and MA-11 were obtained from previous work [21,26]. *Escherichia coli* DH5α (Invitrogen, Carlsbad, CA, USA) and *E. coli* DH5α λpir (Biomedal Life Sciences, Sevilla, Spain) were used for cloning as described previously [21,26]. The strains were maintained as cryo-stocks in 15 % (*v*/v) glycerol at −80 °C. All *P. putida* strains used are listed in Table 1.

2.2. Genetic engineering

Genomic modification of *P. putida* KT2440 was carried out as described previously [27]. The deletion of glucose dehydrogenase (*gcd*, PP_RS07455, previously: PP_1444, NC_002947.4:c1647356-1644945) in *P. putida* MA-1 [28] involved the elimination of the entire open reading frame. For this purpose, approximately 650 bp flanking sequences upstream of the translational start codon (TS1) and downstream of the translational stop codon (TS2) of gcd were amplified from the *P. putida* genome. The amplified sequences were cloned into the *Sma*I linearized vector pEMG via Gibson assembly and subsequently electroporated into *E. coli* DH5αλpir. The created mutant *P. putida* MA-1 *Δgcd* was designated *P. putida* MA-12 after verification by sequencing.

Table 1
Pseudomonas putida strains used in this study.

Strain	Genotype	Reference
KT2440	Wildtype	[111]
MA-1[a]	KT2440 Δ*catBC*	[18]
MA-11[b]	EM42 Δ*catBC* P_{cat} *catA-catA2*	[21]
MA-12[c]	MA-1 *Δgcd*	This work

[a] MA producer strain; accumulation enabled by deletion of muconate cycloisomerase and muconolactone isomerase.

[b] Genome-reduced chassis strain with enhanced catechol conversion via additional expression of catechol 1,2-dioxygenase (CatA2) from the *ben* operon under *Pcat* promoter control (full genotype of EM42 in Table S1).

[c] MA producer strain with disrupted periplasmic glucose oxidation through deletion of glucose dehydrogenase.

2.3. Minimal culture media

The cells were cultivated in minimal glucose medium; the detailed composition is provided in the Supplementary Material. For MA production and tolerance studies, the medium was additionally amended with different stock solutions of benzoate (Sigma–Aldrich, Darmstadt, Germany) and MA (Sigma–Aldrich), whereas the liquid aromatics, including benzaldehyde (Sigma–Aldrich) and benzyl alcohol (Sigma–Aldrich), were added to the medium in pure form. For metabolic flux studies, glucose was replaced with 99 % [1-^{13}C] glucose (Sigma–Aldrich), 99 % [6-^{13}C] glucose (Omicron, Southbend, IN, USA), and an equimolar mixture of naturally labeled glucose and [U-$^{13}C_6$] glucose (Eurisotop, Saint Aubin Cedex, France), respectively [29].

2.4. Chemical depolymerization of polystyrene waste

Polystyrene was depolymerized by photolysis in the presence of *p*-toluenesulfonic acid, yielding crude benzoate that was purified by washing, recrystallization, and optional sublimation. Experimental details on reaction conditions, purification steps, and analytical methods (FTIR, SEC, NMR, GC/MS, HPLC, HPIC) are provided in the Supplementary Material [9].

2.5. Enzymatic depolymerization of textile waste

A textile blend containing 48 % viscose and 52 % polyamide (VI/PA) was purchased from Textil Müller GmbH (Kritzendorf, Austria). For hydrolysis, a Cellic CTec3 cellulase cocktail was purchased from Novozymes (Copenhagen, Denmark). Enzymatic hydrolysis of viscose from the blend was performed in 50 mM potassium phosphate buffer (pH 5.0, 50 °C, 72 h) using 2 % cellulase solution and a solid content of 110 g L^{-1}. After the PA fibers were collected through a 100–500 µm sieve, the viscose hydrolysate was filter sterilized through a 0.2 µm PES filter and further ultrafiltered through a 10 kDa MWCO PES membrane. Monomeric glucose in the final hydrolysate was quantified using HPLC (Agilent Technologies 1260 Infinity II) operated with an Aminex HPX-87H ion exclusion column (Bio-Rad) at 45 °C as the stationary phase, 10 mM H_2SO_4 (0.325 mL min^{-1}) as the mobile phase, and refractive index detection.

2.6. Microbial cultures

For strain characterization, the cells were incubated at 30 °C in baffled shake flasks (10 % filling volume) on an orbital shaker (230 rpm Multitron, Infors-HT, Bottmingen, Switzerland; shaking throw: 25 mm). A single colony from LB agar was used for inoculation of 10 mL of liquid LB medium. The cells were subsequently harvested (6000 ×*g*, 4 min, RT) to inoculate the second preculture and the main culture; both cultures were conducted in 25 mL minimal medium. For MA production, different aromatic compounds were added to the main culture medium. All experiments were conducted in biological triplicate. Tolerance screening was performed in a Biolector bioreactor system as previously described (Beckman Coulter GmbH, Baesweiler, Germany) [21]. In brief, cultivation included one preculture in LB medium, which was used for the inoculation of a second preculture in minimal medium. The main culture was carried out in 48-well flower plates (MTP-48B) with 1 mL of minimal medium supplemented with benzoate, benzaldehyde, or benzyl alcohol (0 to 40 mM). The cultures were inoculated to a starting OD_{600} of 0.5 and grown at 30 °C, 1300 rpm, and a relative humidity of 85 %. The tolerance was evaluated based on the online detected biomass signal (OD_{620}), and both the lag phase and the maximum specific growth rate were considered during the exponential growth phase. Uninoculated medium served as a reference. All experiments were performed in biological triplicate.

2.7. Fed-batch production of MA

The MA production performance of *P. putida* strains was evaluated at 30 °C and pH 7.0 in fed-batch processes at the laboratory scale (1 L DASGIP bioreactors, Eppendorf, Jülich, Germany). The initial batch medium (300 mL) contained 10 g of glucose, 15 g of $(NH_4)_2SO_4$, 7.75 g of K_2HPO_4, 4.25 g of $NaH_2PO_4•2H_2O$, 1 g of $MgCl_2•6H_2O$, 10 mg of EDTA, 10 mg of $FeCl_3•6H_2O$, 1 mg of $CaCl_2•2H_2O$, 1 mL of the abovementioned trace element mixture, and 200 µL of Antifoam 204 (Sigma–Aldrich, Taufkirchen, Germany) per liter of solution [18]. The reactors were inoculated to an initial OD_{600} of 0.1 with the corresponding strain, which was pre-grown and harvested as described above. The initial aeration rate was set to 1 vvm, and pressurized air was used. Later, the dissolved oxygen (DO) level was maintained above 30 % by adjusting the stirrer speed and aeration rate and (when needed) adding pure oxygen. After the batch phase, additional nutrients were supplied through exponential feeding. The concentrated feed contained 600 g of glucose, 50 g of $(NH_4)_2SO_4$, 10 g of $MgCl_2•6H_2O$, 50 mg of EDTA, 50 mg of $FeCl_3•6H_2O$, 5 mg of $CaCl_2•2H_2O$, 10 mL of the abovementioned trace element mixture, and 200 µL of Antifoam 204 (Sigma–Aldrich) per liter of solution. For each setup, the feed profile was programmed using VBA scripting, which was built in DASGIP control software. Two process strategies were applied. The basic strategy included an exponential glucose feed, which was based on the desired specific growth rate ($\mu_{set} = 0.04\ h^{-1}$), the biomass yield on glucose ($Y_{X/S}$), the maintenance energy requirement (m_s), and the increasing liquid volume (V_L) (Eq. 1):

$$F = \left(\frac{\mu_{set}}{Y_{x/S}} + m_s\right) \bullet \frac{V_L X_0 e^{\mu_{set}\ (t-t_0)}}{S_0} \quad (1)$$

The other parameters were the reactor liquid volume V_L, the biomass concentration at the beginning of the feed phase X_0, and the glucose concentration of the feed S_0. The addition of benzoate was coupled with the automatic pH control (pH-stat) [30,31]. Two feed solutions were tested. One contained 1.2 M benzoate and 2.4 M NaOH (resulting in more frequent benzoate pulses), and the other contained 1.2 M benzoate and 2.88 M NaOH (resulting in less frequent benzoate pulses). In an advanced set-up, different amount of glucose and benzoate were supplied (Eq. 2). For glucose supplementation after the batch phase, an exponential feed was used, and an increasing maintenance requirement over time was considered.

$$F = \left(\frac{\mu_{set}}{Y_{x/S}} + m_s \bullet e^{0.02\ (t-t_0)}\right) \bullet \frac{V_L X_0 e^{\mu_{set}\ (t-t_0)}}{S_0} \quad (2)$$

The addition of benzoate, which started during the glucose-feed phase, was coupled to the dissolved (DO) signal. Once the DO level surpassed a predefined setpoint (50 %), benzoate was automatically added from the concentrated feed until a concentration of 5 mM or 10 mM was reached. For exponential glucose feeding, experimentally obtained growth parameters were considered for each strain: MA-1 and MA-12 $Y_{X/S} = 0.40\ g\ g^{-1}$, $m_s = 0.037\ g\ g^{-1}\ h^{-1}$; MA-11 $Y_{X/S} = 0.55\ g\ g^{-1}$, $m_s = 0.024\ g\ g^{-1}\ h^{-1}$ [32]. All fermentations were conducted in duplicate.

2.8. Fed-batch MA production from polystyrene-upcycled benzoate

Through photolysis, 5.75 g of crude benzoate was extracted from polystyrene. The resulting powder was then dissolved in water, and the pH was adjusted to 12.0 using 6 M NaOH. The measured concentration of benzoate in the solution was 1.0 M. The production of MA from upcycled benzoate was demonstrated using *P. putida* MA-11 under fed-batch conditions at 30 °C and pH 7.0 in a 100 mL scale system (DASGIP, Eppendorf, Jülich, Germany). The initial batch medium (100 mL) contained 10 g of glucose, 15 g of $(NH_4)_2SO_4$, 7.75 g of K_2HPO_4, 4.25 g of $NaH_2PO_4•2H_2O$, 1.0 g of $MgCl_2•6H_2O$, 10 mg of EDTA, 10 mg of $FeCl_3•6H_2O$, 1 mg of $CaCl_2•2H_2O$, 1 mL of the abovementioned trace element solution, and 200 µL of Antifoam 204 (Sigma–Aldrich, Taufkirchen, Germany) per liter of solution [18]. The reactor was inoculated to an initial OD_{600} of 0.1, and an initial aeration rate was set at 1 vvm using pressurized air. To maintain the dissolved oxygen (DO) level above 30 %, the stirrer speed and aeration rate were adjusted as needed, and pure oxygen was added when necessary. Following the batch phase, additional glucose was supplied through exponential feeding from a concentrated stock (Eq. 2). Benzoate was fed in pulses, triggered by an increase in the DO signal. Owing to the limited availability of upcycled benzoate, the process was conducted as a single replicate.

2.9. Quantification of the cell concentration, substrates and products

The cell concentration was monitored spectrophotometrically at 600 nm (OD_{600}) (VWR). A correlation factor of 0.54 $g_{CDW}\ L^{-1}\ OD_{600}^{-1}$ was used for the conversion of OD_{600} readings into dry cell weights (DCWs) [26]. Glucose was quantified using isocratic HPLC (1260 Infinity Series, Agilent, Darmstadt, Germany) with a MetaCarb 87C guard column (50 × 4.6 mm, Agilent) and a MetaCarb 87C analytical column (300 × 7.8 mm, 9 µm, Agilent) at 85 °C as the stationary phase, deionized water at a flow rate of 0.6 mL min^{-1} as the mobile phase, and refractive index detection (Agilent 1260 RID G1362A, Agilent Technologies). Gluconate and 2-ketogluconate were quantified using HPLC as described previously [21]. Aromatics and MA were analyzed using HPLC (1260 Infinity Series, Agilent Technologies) using a modified gradient method [33]. Experimental details on separation conditions, detection, and calibration are provided in the Supplementary Material.

2.10. In-vivo degradation assays of benzoate and catechol

Cells, pre-grown in in glucose-medium in the presence of 5 mM and 25 mM benzoate, as well as without benzoate were analyzed for their capacity to degrade benzoate and catechol. For this purpose, cells were harvested from the pre-cultures and incubated at a cell concentration of about 0.25 g (cell dry mass) L^{-1} in glucose-medium, supplemented with either 5 mM benzoate or 2.5 mM catechol as the degradation substrate. The degradation rate was determined by monitoring the linear decline of the concentration of the corresponding substrate every 10 min over a period of 60 min [18]. The obtained rate was then corrected for the mean cell concentration during the incubation period, which yielded the specific degradation rate (mmol $g^{-1}\ h^{-1}$). All experiments were conducted as three biological replicates.

2.11. In-vitro activity of catechol 1,2-dioxygenase

The activity of catechol 1,2-dioxygenase was measured as described previously [34]. The specific enzyme activity was given in U (mg cell protein)$^{-1}$.

2.12. Isotopic tracer studies and ^{13}C labeling analysis

Precultured and washed cells (see above) were transferred to 25 mL of ^{13}C tracer medium; here, the initial cell concentration was kept below $OD_{600} = 0.02$ to exclude the interference of unlabeled biomass with the subsequent ^{13}C labeling analysis [35]. To resolve the biochemical network of *P. putida*, parallel setups containing [1-^{13}C] glucose, [6-^{13}C] glucose, and an equimolar mixture of naturally labeled glucose and [U-$^{13}C_6$] glucose as tracer substrates were used [29]. The three replicates yielded the physiological parameters related to growth, glucose consumption and organic acid secretion rates. During exponential growth (OD_{600} 2–5), the cells were harvested for ^{13}C analysis of the amino acids from the cell proteins as well as sugars from the cell carbohydrates [29]. Harvested cells from the isotopic tracer studies (2 mg CDW) were washed with deionized water, followed by hydrolysis in 100 µL of 6 M HCl (24 h, 100 °C). The proteinogenic amino acids contained

in the hydrolysates were derivatized into the corresponding *t*-butyl-dimethyl-silyl derivatives, and their ^{13}C labeling pattern was analyzed using GC/MS as described previously [36]. Additionally, GC/MS was applied to obtain ^{13}C labeling data for cellular sugars [29].

2.13. Metabolic flux estimation and redox and energy balance

Metabolic fluxes in the metabolic network of *P. putida* (Table S2) were estimated from the experimental data (Table 2) and the cellular composition [37], yielding the anabolic precursor demand (Table S3) using OpenFLUX software [38] integrated into MATLAB (MathWorks, Natick, USA) [29]. Prior to estimation, the obtained mass isotopomer distributions were corrected for naturally occurring isotopes [39] using a built-in algorithm of OpenFLUX. Because the nonlinear structure of isotopomer models potentially leads to local minima, 100 parameter estimations with random initial starting points were performed. These yielded the same solution and verified that the acquired data were descriptive and that the determined flux distribution displayed the global minimum [29] (Table S4). After flux parameter estimation, 95 % confidence intervals were determined over 100 iterations using Monte Carlo analysis [40]. Generally, an excellent fit of the data was obtained (Table S5, Fig. S1). Details on the calculation of balances for reducing equivalents and energy equivalents from the estimated fluxes are given in the Supplementary Material.

2.14. RNA sequencing

Transcriptomic analysis was conducting using RNA sequencing. Experimental details are provided in the Supplementary Material.

2.15. Recovery, purification, and quality analysis of fermentative MA

Downstream processing was adapted from previous work [18]. Experimental details are provided in the Supplementary Material.

2.16. Chemical synthesis of nylon-6,6 precursors and PA66

Adipic acid was synthesized from fermentative MA via catalytic hydrogenation [18] using 2-methyltetrahydrofuran as a green solvent, followed by conversion into 1,6-hexanediol [41] and hexamethylenediamine [42] through established reduction routes. Both commercial and MA-derived intermediates were tested, and the final products were confirmed by NMR and melting point analysis. Experimental details on reaction conditions, purification, and product characterization are provided in the Supplementary Material. Fully waste-based PA66 was synthesized from hexamethylenediamine and adipic acid using a two-step melt and solid-state polymerization procedure. For comparison, petrochemical PA66 was prepared from commercial precursors using the same method. Experimental details on polymerization conditions and PA66 characterization are provided in the Supplementary Material.

3. Results

3.1. Benzoate and its derivatives are promising polystyrene-derived monomers for MA production in P. putida MA-1

Benzoate [7–9] and benzaldehyde [8,10,43] can be obtained using chemo-catalytic polystyrene depolymerization and can be further transformed into benzyl alcohol via microbial processes [44]. To assess the strain's performance, *P. putida* MA-1 [26] was evaluated for its tolerance to and utilization of these aromatic compounds (Fig. S10). The strain exhibited robust growth in benzoate concentrations up to 10 mM, with no effect on the growth rate, lag phase, or biomass formation, indicating high resilience. At higher concentrations, growth slowed, with a half-maximal inhibitory concentration (IC) of 28.5 mM, and the biomass decreased at concentrations near 30 mM. The strain showed better tolerance to benzaldehyde (IC = 32.1 mM), but its lag phase was extended at elevated concentrations, indicating detoxification mechanisms. Benzyl alcohol was found to be more inhibitory, with lower biomass formation and a reduced IC. Despite slower growth at high aromatic concentrations, the growth substrate glucose was consistently consumed in all cases. The byproduct profile varied with the presence of the aromatic compounds: with 30 mM benzoate, 60 % of the glucose was converted into 2-ketogluconate (Fig. S11). In contrast, up to 30 mM benzaldehyde led to complete glucose metabolism without byproducts; this was correlated with increased biomass. At 40 mM benzaldehyde, gluconate production increased. Benzyl alcohol also triggered 2-ketogluconate formation, although at a lower yield (30 %). The screening demonstrated the exceptional natural ability of the bacterium to tolerate polystyrene-derived aromatic monomers; this bacterium showed a notably greater tolerance than other industrially significant aromatics, such as catechol, a major lignin-derived monomer [21].

For MA production, 5 mM benzoate and 7.5 g L^{-1} glucose (growth substrate) enabled complete conversion of benzoate to MA within only two hours, demonstrating efficient substrate utilization (Fig. 1A). Benzaldehyde was also converted into MA, although more slowly (12*h*), due to initial reduction into benzyl alcohol (40 % of the substrate) and partial oxidation to benzoate (30 %) (Fig. 1B). This pattern resembled the native detoxification mechanisms observed in other bacteria [33]. Once benzaldehyde was depleted, the remaining benzoate was rapidly metabolized. The final step involved the oxidation of benzyl alcohol back to benzaldehyde and subsequently to benzoate to complete the process. Notably, glucose depletion at seven hours reduced the metabolic activity, likely prolonging the conversion. Benzyl alcohol was also a viable MA precursor, and the strain exhibited biphasic metabolism (Fig. S12). In the presence of glucose, benzyl alcohol was weakly converted into MA with no byproducts. After glucose depletion, its consumption accelerated, significantly increasing MA yields. Additionally,

Table 2
Physiology of the different glucose-grown *P. putida* strains in the presence of increased levels of benzoate (BA) and MA. The data represent rates and yields for the wild type (KT2440) and the MA-producing derivatives MA-1 (KT2440 Δ*catBC*) and MA-12 (MA-1 Δ*gcd*), estimated during the exponential growth phase. The net carbon uptake rate (q_S) reflects the difference between the glucose consumption (q_{Glc}) and the secretion of gluconate (q_{GA}) and 2-ketogluconate (q_{2KGA}). In addition, the specific growth rate (μ) and the corresponding biomass yield of consumed glucose ($Y_{X/Glc}$) and net-consumed carbon ($Y_{X/S}$) are provided. Glucose-based cultures without extra addition served as controls. The data represent the mean values and standard deviations from three biological replicates.

Strain	Extra addition	μ [h^{-1}]		q_{Glc} [mmol g^{-1} h^{-1}]		q_S [mmol g^{-1} h^{-1}]		$Y_{X/Glc}$ [g mol^{-1}]		$Y_{X/S}$ [g mol^{-1}]		q_{GA} [mmol g^{-1} h^{-1}]		q_{2KGA} [mmol g^{-1} h^{-1}]	
KT 2440	–	0.55	± 0.02	6.76	± 0.23	6.10	± 0.21	81.6	± 7.8	90.6	± 4.3	0.59	± 0.03	0.06	± 0.01
MA-1	–	0.53	± 0.02	6.63	± 0.19	6.24	± 0.11	80.1	± 6.1	85.4	± 3.0	0.27	± 0.07	0.12	± 0.06
	5 mM BA	0.47	± 0.03	5.75	± 0.23	5.22	± 0.36	82.2	± 4.1	89.8	± 8.2	0.35	± 0.07	0.18	± 0.06
	25 mM BA	0.36	± 0.03	7.03	± 0.38	5.17	± 0.23	51.7	± 4.4	69.5	± 5.8	0.72	± 0.24	1.14	± 0.30
	50 mM MA	0.54	± 0.01	6.52	± 0.23	6.01	± 0.06	83.1	± 3.6	90.3	± 1.9	0.30	± 0.07	0.22	± 0.02
	300 mM MA	0.24	± 0.02	5.58	± 0.13	3.20	± 0.17	46.7	± 5.1	75.2	± 8.6	0.42	± 0.06	1.97	± 0.22
MA-12	–	0.34	± 0.02	4.75	± 0.18	4.75	± 0.18	72.8	± 6.2	72.8	± 6.2	n. d.		n. d.	

n.d. = not detected.

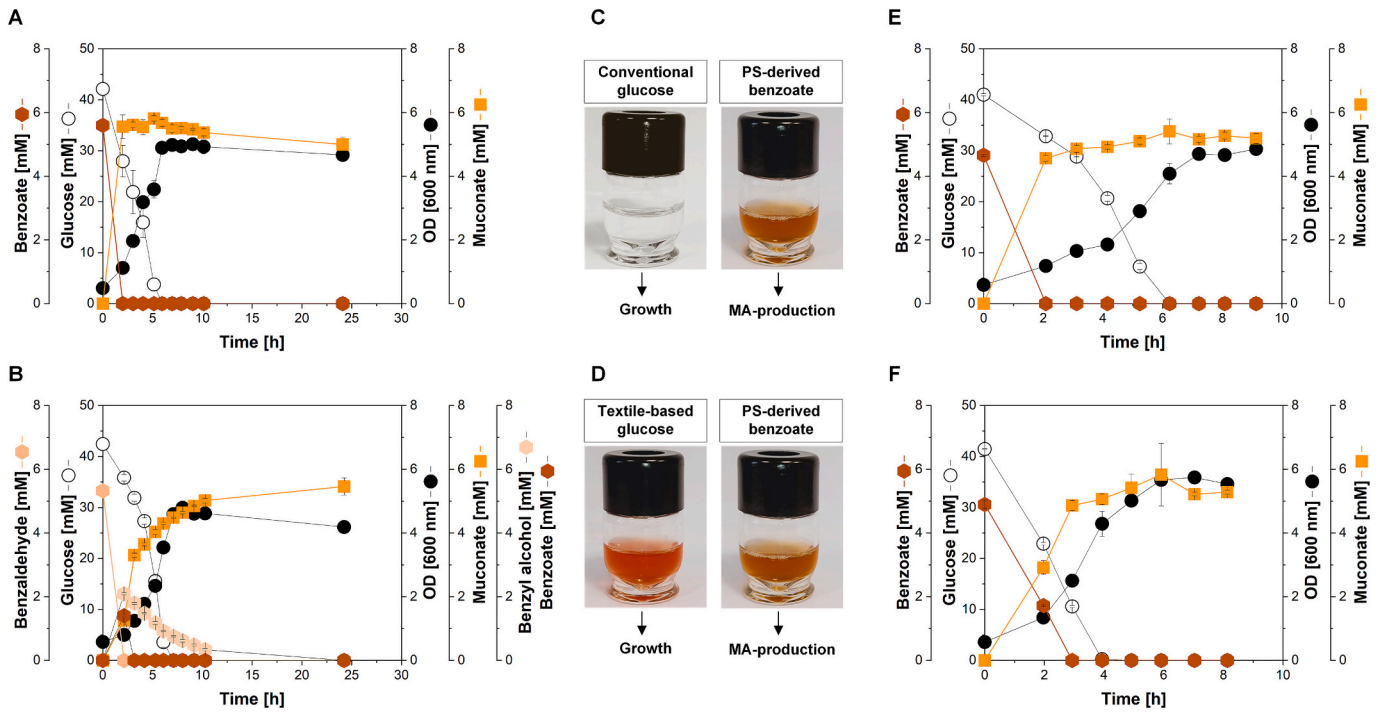

Fig. 1. Upcycling of polystyrene-derived benzoate to MA using *P. putida* MA-1. Evaluation of MA production in shake flasks using minimal medium supplemented with 5 mM benzoate (A) or 5 mM benzaldehyde (B) as biotransformation substrates, and 7.5 g L^{-1} glucose as the growth substrate. $n = 3$. MA production from 5 mM polystyrene-derived crude benzoate as the biotransformation substrate and 7.5 g L^{-1} glucose as the growth substrate (C, D). The glucose source was either commercially obtained (C) or derived from the enzymatic hydrolysis of a viscose–polyamide textile blend, yielding a glucose-rich hydrolysate (D). $n = 3$.

the exclusive formation of MA without intermediates indicated efficient channeling of the aromatic compound. Overall, benzoate emerged as the most favorable substrate because of its superior tolerability, rapid conversion, and minimal byproduct formation. These results highlighted *P. putida* MA-1's potential for upgrading polystyrene-associated aromatic monomers into valuable biochemical products.

3.2. Upcycling of polystyrene-derived benzoate and textile-based glucose enables sustainable MA production

We performed light-induced oxidative cleavage of commercial polystyrene with *para*-toluenesulfonic acid monohydrate (pToS) under 405 nm irradiation; this process resulted in efficient polymer degradation. The reaction was conducted in an autoclave with stirring and produced benzoic acid in yields consistent with prior reports [28]. SEC analysis revealed a rapid reduction in the polymer molar mass from ~200 to 50 kg mol^{-1} within one hour, and 49 kg mol^{-1} was reached after 3.5 h (Fig. S13). Depolymerization slowed in later stages. Post-extraction and drying yielded 1.2 g of crude benzoic acid as a light brown powder. Subsequent sublimation produced high-purity white benzoic acid crystals, with some material loss (crude: 68.4 ± 1.2 % purity; sublimated: 101.4 ± 2.4 % by HPLC). We then assessed *P. putida* MA-1 for its ability to convert crude polystyrene-derived benzoate (5 mM) directly into MA, using glucose (7.5 g L^{-1}) as a growth substrate (Fig. 1C). Remarkably, the conversion was completed within two hours, matching the performance of commercial benzoate (Fig. 1E). MA purified from the culture supernatant was equivalent in purity to that from commercial sources.

To enhance sustainability, we substituted the glucose source with an enzymatically hydrolyzed viscose from a red-colored viscose-polyamide textile blend [45]. After viscose hydrolysis and polyamide removal, the resulting solution provided a glucose-rich hydrolysate (50 g L^{-1}). The cultivation of *P. putida* MA-1 with polystyrene-derived crude benzoate and textile-derived hydrolysate (7.5 g L^{-1} glucose) (Fig. 1D) led to full benzoate consumption within three hours, yielding the first fully waste-based MA (Fig. 1F). *P. putida* MA-1 also successfully converted sublimated benzoate originating from polystyrene in the presence of both conventional and textile-derived glucose (Fig. S14). Notably, the growth was faster on the waste-derived glucose than on conventional glucose. Previously, glucose-rich hydrolysates were found to support robust microbial growth, and this observation suggests that additional components in the hydrolysate may contribute to enhanced performance [46,47]. Such effects may be attributed to additional compounds released from the textile blend during hydrolysis, such as short peptides, or trace minerals, which could act as supplementary nutrients or growth enhancers. Further investigation is warranted to identify and characterize these potential growth-promoting factors.

3.3. Systems-level evaluation of metabolic bottlenecks: ^{13}C flux analysis under benzoate stress

At elevated benzoate concentrations, growth suppression and reduced cell vitality were observed (Fig. S10); these results highlighted potential challenges for fermentative production processes that rely on benzoate over extended periods. To identify metabolic bottlenecks and inform bioprocess optimization, we performed ^{13}C metabolic flux analysis and employed isotopic tracers to comprehensively map the carbon flux distribution and pathway activity in living cells [29]; these results provided critical insights into the dynamic metabolic adaptations under stress [48–52].

Under the control conditions (glucose alone), *P. putida* MA-1 predominantly utilized periplasmic gluconate bypass (51 % of glucose uptake), followed by the cytosolic glucose-phosphorylating route (39 %), with marginal flux through the 2-ketogluconate loop (3 %) (Fig. S15). These pathways converged at 6-phosphogluconate (6PG) and fed the Entner-Doudoroff (ED) pathway to generate glyceraldehyde-3-phosphate (GAP) and pyruvate (PYR). PYR was converted to acetyl-CoA to fuel the highly active tricarboxylic acid (TCA) cycle (85 % flux), whereas part of the GAP pool was recycled into sugar phosphates for anabolism. Upon exposure to 5 mM benzoate, central carbon fluxes

remained largely stable, with minor reductions in the ED pathway, pyruvate carboxylase, and malic enzyme fluxes (Fig. S16A). The NADPH-forming malic enzyme and ATP-consuming pyruvate carboxylase created an alternative pathway to the NADH-forming malate dehydrogenase for converting malate into oxaloacetate, thereby balancing ATP, NADH, and the NADPH supply. A reduction in the bypass activity indicated a metabolic shift favoring energy conservation at the cost of NADPH availability. Despite this shift, benzoate conversion to MA remained highly efficient (88 % flux) through benzoate and catechol dioxygenases (B12DO, C12DO).

At 25 mM benzoate, the flux redistribution became pronounced (Fig. 2A). While glucose uptake remained high, biomass yields declined by 40 %, and specific growth rates decreased by 35 %; these results indicated reduced anabolic efficiency (Table 2). The flux of benzoate-to-MA conversion sharply decreased by more than elevenfold to just 8 %. Energy-intensive cytosolic glucose assimilation was downregulated, whereas periplasmic glucose oxidation significantly increased. This shift led to the release of gluconate and 2-ketogluconate, which together accounted for 26 % of the loss of assimilated carbon. Concurrently, the TCA cycle flux increased by 11 %. Despite the altered flux distribution, the NADPH supply remained stable because of a substantial redistribution of the pathway contributions (Fig. 2B, Fig. S17A, Fig. S17C). The reduced NADPH generation from G6P dehydrogenase was compensated by increased flux through ICD dehydrogenase and malic enzyme.

3.4. Transcriptional and metabolic profiling of the benzoate degradation pathway

To further investigate the functional consequences of these metabolic shifts, we conducted in-vivo benzoate and catechol degradation assays using *P. putida* MA-1 pre-cultivated under varying benzoate stress conditions (0, 5, 25 mM benzoate) (Fig. 3C). The short incubation time excluded the possibility of interference from newly synthesized proteins, ensuring that the measured degradation capacity reflected the physiological state and enzymatic potential of the cells during the pre-incubation phase [18]. Non-induced control cells (0 mM benzoate) efficiently degraded catechol, attributed to basal expression of *catA*, which encodes catechol 1,2-dioxygenase [20]. With increasing benzoate pre-exposure, catechol degradation capacity increased six-fold, correlating with induction of the *ben* operon, which includes *catA2*—a second catechol 1,2-dioxygenase gene in *P. putida* [18]. These results aligned with in vitro catechol 1,2-dioxygenase activity assays, which also showed increasing enzyme activity with higher stress levels (Fig. 3D). In contrast, in-vivo benzoate degradation declined sharply under high stress. The specific benzoate degradation rate dropped from 5.6 mmol g^{-1} h^{-1} at 5 mM benzoate to 0.4 mmol g^{-1} h^{-1} at 25 mM. In all cases, the catechol conversion capacity was significantly higher than the benzoate conversion capacity, likely to ensure that no toxic pathway intermediates accumulate inside the cell.

To elucidate the transcriptional basis of the reduced benzoate degradation capacity under stress, RNA sequencing was performed on *P. putida* MA-1 grown in the presence of 5 mM and 25 mM benzoate and without benzoate, used as a control. Genes of the *ben* (*benABC, benD, catA2*) and the *cat* operon (*catA*) were found induced in the presence of 5 mM benzoate (Fig. 3A), well matching previous findings [34]. Under high-stress conditions, the benzoate importers *benE* and the *benF*-like outer membrane porin PP_1383, as well as *catA2*, were downregulated. In contrast, *benABC* and *benD* were found to be upregulated (Fig. 3B). Apparently, under high benzoate stress, *P. putida* undergoes a regulatory shift that decoupled benzoate uptake from downstream catechol degradation. This selective regulation might reflect a stress-adaptive response prioritizing intracellular detoxification over substrate assimilation. More research is needed to resolve this picture in more detail.

Altogether, the metabolic adjustments enabled cells to manage the elevated stress but resulted in suboptimal glucose utilization, increased byproduct formation, and reduced MA production. These findings indicated that increased benzoate levels resulted in energy-inefficient metabolism; therefore, maintaining benzoate at lower concentrations during fermentation was crucial for enabling energy-efficient glucose utilization in strain MA-1.

3.5. Metabolic constraints and flux adaptations under MA stress

At elevated concentrations, MA significantly inhibited *P. putida* MA-1 growth (Fig. S10). Since achieving high product titers is a crucial factor for industrial process optimization, addressing this inhibitory effect was essential. From a biochemical standpoint, both benzoate and MA are weak acids that may disrupt cellular energy homeostasis by uncoupling the transmembrane proton gradient from ATP synthesis [53]. To systematically assess the impact of MA stress on metabolic flux distribution, we conducted ^{13}C metabolic flux analysis under moderate (50 mM) and high (300 mM) MA concentrations, and the latter was in the range of top MA titers from benzoate.

At 50 mM MA, metabolic flux adjustments were localized primarily around the pyruvate (PYR) node and closely resembled the response observed under mild benzoate stress (Fig. S16). However, at 300 mM MA, carbon metabolism was globally perturbed (Fig. 2C). Periplasmic glucose oxidation increased, whereas cytosolic glucose uptake was severely suppressed. More than 40 % of the assimilated glucose was rerouted into gluconate and 2-ketogluconate, whereas all three cytosolic carbon uptake routes were downregulated; this drastically limited the flux available for downstream biosynthesis. This disruption led to substantial reductions in the Entner–Doudoroff by restricting the (ED) pathway, the EDEMP cycle, and the TCA cycle fluxes and severely impaired both ATP generation and NADPH production. As a result, the cellular energy and redox power supply decreased by one-third (Fig. 2D); these results highlighted the inability of *P. putida* MA-1 to effectively compensate for high MA-induced stress.

Thus, the combined exposure to elevated substrate (benzoate) and product (MA) concentrations would likely intensify the metabolic stress. High levels of benzoate and MA shift the metabolism of excess glucose toward periplasmic oxidation and increased byproduct secretion. To mitigate these effects, fermentation strategies need to prioritize optimized glucose flux partitioning and minimized byproduct formation to sustain metabolic efficiency under inhibitory conditions.

3.6. Precision fermentation approach: optimized glucose and benzoate feeding for efficient MA production

Benzoate and MA significantly disrupted the metabolism of *P. putida* MA-1, highlighting the need for a strategic approach to sustain high-level MA production over extended fermentation periods. To evaluate these metabolic effects and develop optimized process strategies, we conducted three fed-batch fermentations in laboratory-scale bioreactors.

Glucose supplementation began after the batch phase using an exponential feed rate (Eq. 1), and this feed rate remained consistent across all experiments. Benzoate was supplied pulse-wise, triggered by pH fluctuations, following an approach based on proton release associated with aromatic compound conversion into MA [30]. In one experiment, benzoate and NaOH were added at a 1:2 ratio (1.2 M benzoate, 2.4 M NaOH) to precisely match the theoretical conversion stoichiometry. In addition, an increased 1:2.4 ratio (1.2 M benzoate, 2.88 M NaOH) was applied to counteract the additional acidification caused by gluconate and 2-ketogluconate formation (Fig. 5) and the proton release linked to ammonium assimilation [31]. A control fermentation without benzoate feeding was also included to assess baseline metabolic performance.

Benzoate addition had a strong effect on the growth of strain MA-1 (Fig. S18). In the control process, the cells reached an OD_{600} of 50 after 68 h; this value was twice the OD_{600} of the benzoate-supplied, MA-producing cells that received the same amount of glucose. The reduced growth indicated that glucose was diverted away from biomass

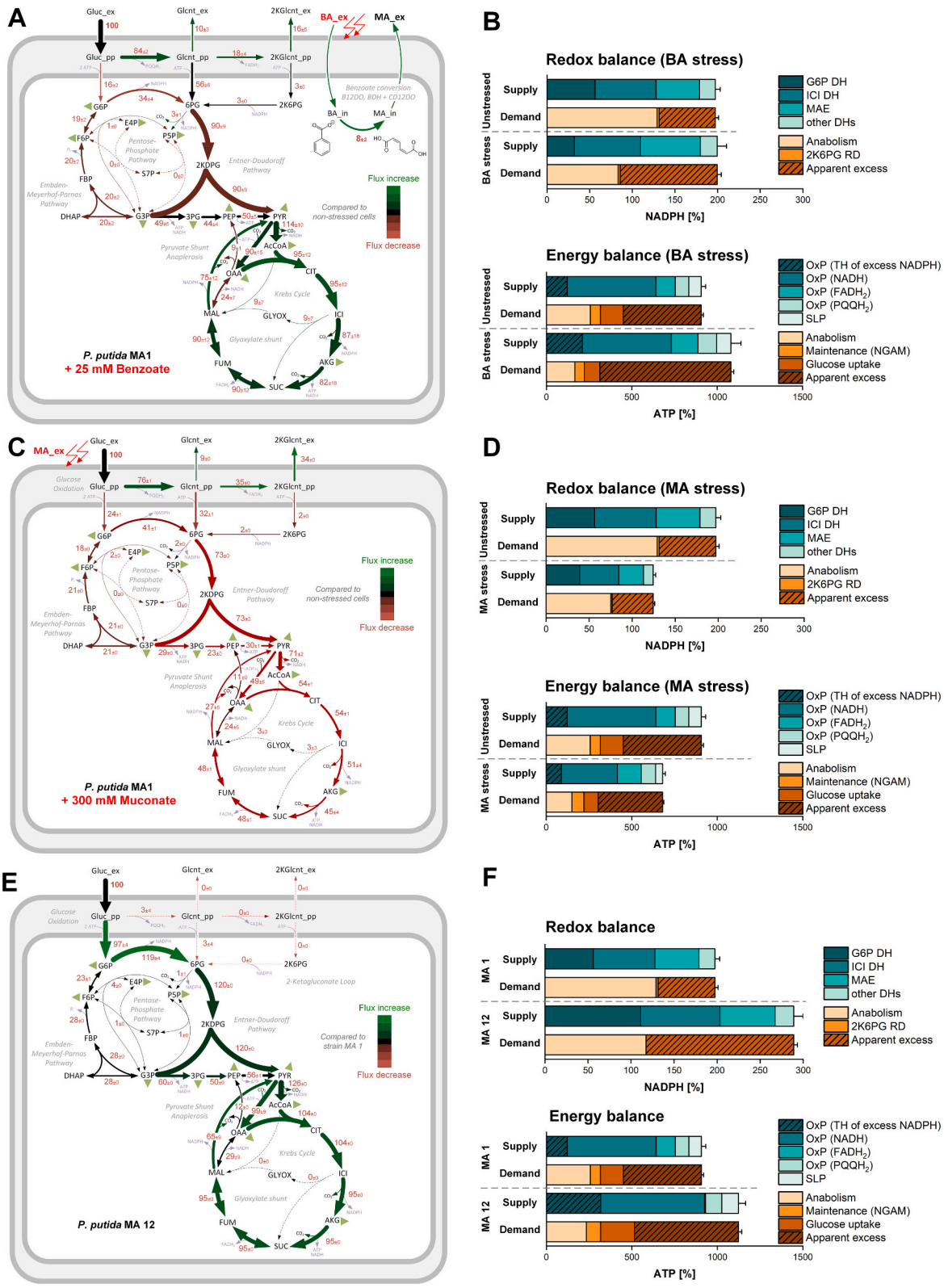

Fig. 2. Carbon flux distribution across different *P. putida* strains as determined by ^{13}C metabolic flux analysis. Intracellular carbon fluxes of glucose-grown *P. putida* MA-1 in the presence of 25 mM benzoate (A) and 300 mM MA (C). Intracellular carbon of glucose-grown *P. putida* MA-12 (*P. putida* MA-1 *Δgcd*) (E). All fluxes are expressed as a molar percentage relative to the specific glucose uptake rate (q_S), which was set to 100 % (Table 2). Biomass formation reactions are represented by green triangles, with their flux values available in Supplementary File 1. Flux differences between the conditions are visually indicated by color gradients; here, higher fluxes appear from dark to light green and lower fluxes from dark to light red relative to the control. The corresponding NADPH and ATP balances (B, D, F) are derived from carbon flux distributions, illustrating metabolic sources and cellular sinks. Abbreviations: G6P DH – glucose 6-phosphate dehydrogenase; ICI DH – isocitrate dehydrogenase; MAE – malic enzyme; DH – dehydrogenase; 2K6PG RD – 2-keto-6-phosphate gluconate reductase; OxP – oxidative phosphorylation; SLP – substrate-level phosphorylation; TH – transhydrogenation; NGAM – non-growth-associated maintenance. An apparent excess or oversupply of NADPH or ATP is obtained from the difference between the summed-up supply and the quantifiable demand.

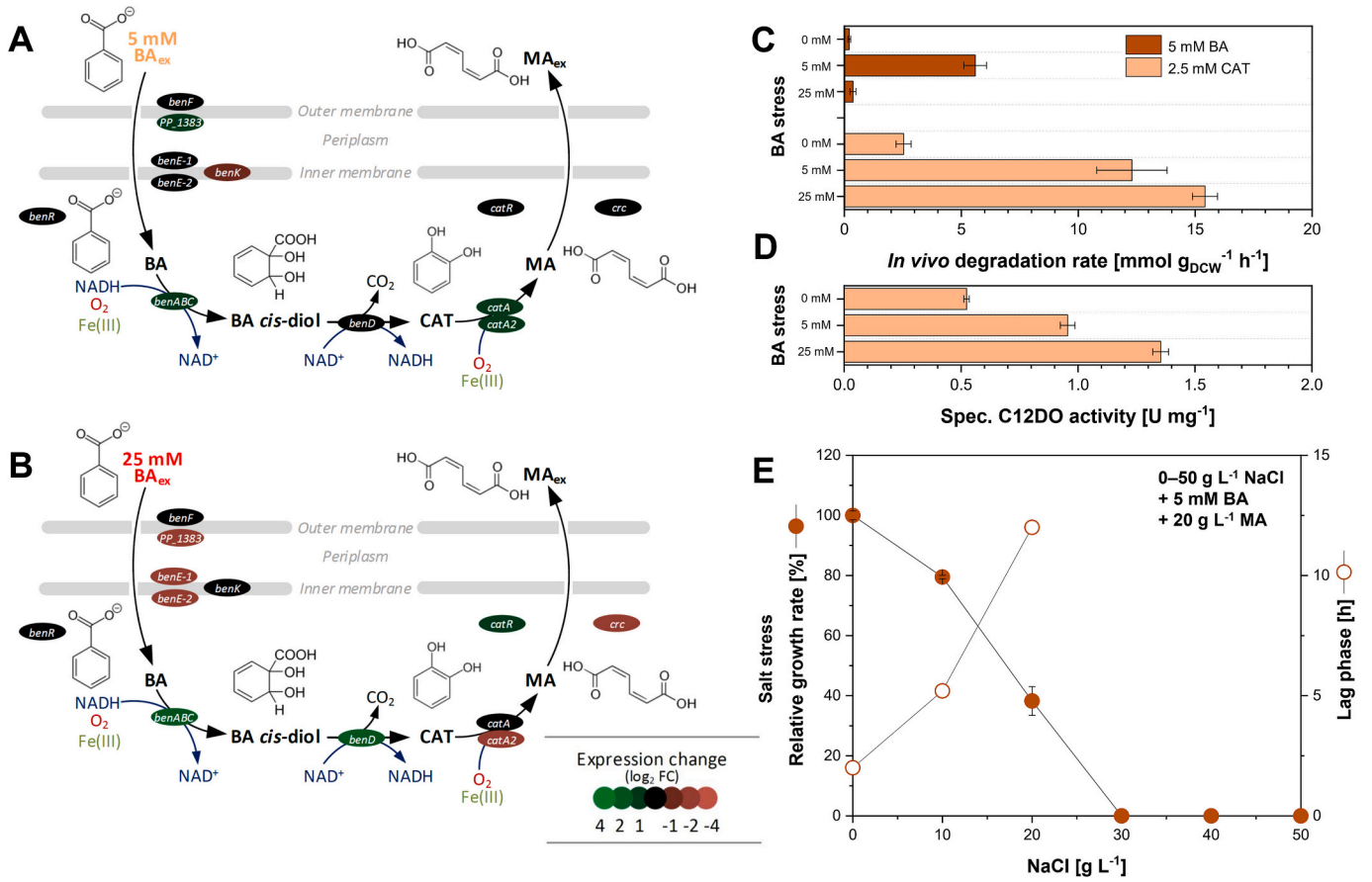

Fig. 3. Transcriptional and metabolic profiling of the benzoate degradation pathway in *P. putida* MA-1 under benzoate and salt stress. (A, B) Gene expression related to benzoate uptake and conversion to muconic acid (MA) was analyzed by RNA sequencing ($n = 3$). Cells were cultivated with 5 mM (A) and 25 mM (B) benzoate, alongside a no-benzoate control. Data are presented as $\log_2$-fold changes relative to the control condition. (C) In vivo benzoate and catechol degradation rates were measured following pre-growth in the presence of 0, 5, or 25 mM benzoate ($n = 3$). (D) The in vitro activity of catechol 1,2-dioxygenase was quantified under the same stress conditions ($n = 3$). (E) Salt tolerance of strain MA-1 was assessed across a NaCl gradient (0–50 g L^{-1}) using a microbioreactor system ($n = 3$). The glucose-medium medium additionally contained 5 mM benzoate and 20 g L^{-1} MA. Experimental details are described in Fig. 1.

formation. This observation was consistent with previous flux data, which showed that high benzoate levels led to increased periplasmic glucose oxidation and byproduct secretion, redirecting carbon away from energy-efficient central pathways (Fig. 2). As the process progressed, this effect intensified, indicating that cells required increasing amounts of energy to sustain activity under inhibitory conditions and that the available glucose became insufficient.

3.7. High-level fed-batch production from benzoate using P. putida MA-1 and its genome-reduced derivative MA-11

To address this challenge, a dynamic control strategy for fermentative MA production was designed to account for the increasing maintenance energy demand. This approach involved supplying progressively higher amounts of glucose over time to counteract the increasing inhibitory effects (Eq. 2). Since the conversion of benzoate to MA requires two oxygen-consuming dioxygenases, the dissolved oxygen (DO) level was identified as suitable online sensor for benzoate availability rather than using the pH; the use of the pH value was found suboptimal because of the fixed ratio of base to benzoate in the feed. Consequently, benzoate addition was correlated to the DO signal to ensure that substrate availability aligned with the metabolic capacity of the cells.

The designed dynamic process concept, incorporating maintenance energy-corrected glucose feeding and DO-based benzoate feeding, was first applied for high-level MA production in stirred tank bioreactors using *P. putida* MA-1 (Fig. 4A). During the batch phase, the strain exhibited robust growth and reached an OD_{600} of 3 after 6 h. At this point, 10 mM benzoate was added to induce the expression of catabolic pathways. Upon glucose depletion at 12 h, the exponential glucose feed commenced and was adjusted to account for the increasing maintenance energy requirements over time (0.037 g $(g_{DCW})^{-1}$ h^{-1}). The target growth rate was maintained at $\mu_{set} = 0.04$ h^{-1} to prevent excessive oxygen demand that could compete with MA biosynthesis.

Once the cell density reached an OD_{600} of 15, which occurred after 24 h, the automatic DO-coupled benzoate feed (5 mM pulses) was initiated. Each benzoate pulse triggered a drop in the DO level, indicating active conversion of the aromatic substrate to MA. As soon as the benzoate was metabolized, the DO levels sharply increased, signaling that the system should administer the next feed pulse. This setup ensured a steady but low benzoate concentration throughout the process, maintaining metabolic stability and enabling increased efficiency.

For the next 36 h, the volumetric productivity remained stable at 1.6 g L^{-1} h^{-1} and gradually declined toward the end of the process. After 80 h, a final titer of over 65 g L^{-1} MA was achieved. Importantly, the accumulation of unwanted byproducts was minimal throughout the process. Only gluconate and 2-ketogluconate were detected, both at low concentrations (< 1 g L^{-1}). The alternative supply of 10 mM benzoate pulses resulted in comparable performance. Doubling the pulse size and halving the frequency maintained the same productivity, highlighting the robustness of the process to variations in the feed dynamics (Fig. S19).

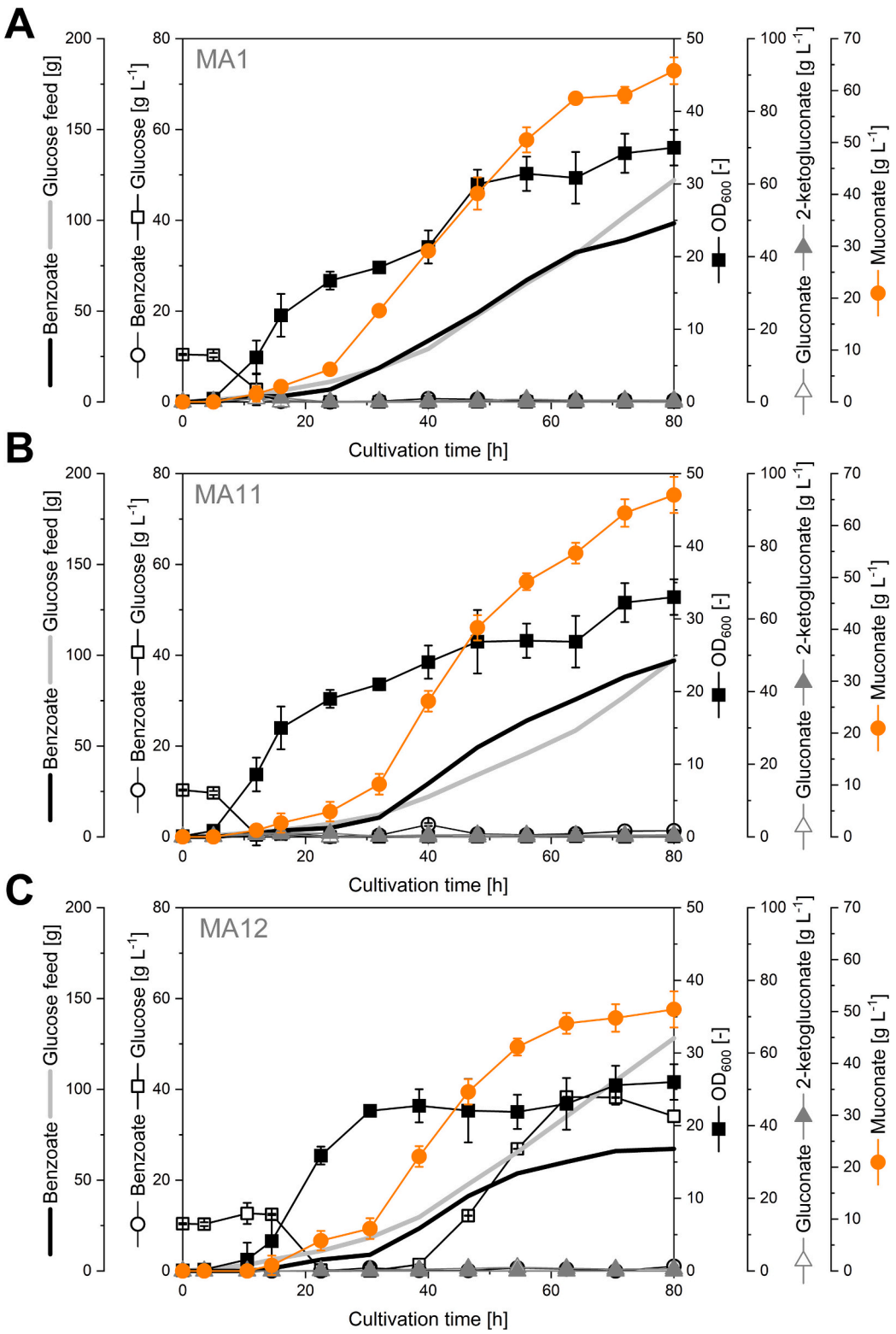

Fig. 4. DO-based fed-batch production of MA from benzoate using *P. putida* MA-1 (A), MA-11 (B), and MA-12 (C). The cells were grown in glucose minimal medium under exponential feeding. The automatic addition of 5 mM benzoate pulses was triggered by an increase in the dissolved oxygen level, indicating the complete conversion of the previous dose via benzoate and catechol dioxygenases.

To further validate this process, the same feeding strategy was applied to *P. putida* MA-11, which is a genome-reduced derivative optimized for metabolic efficiency. Based on the observed metabolic impact of benzoate and MA (Fig. 2), strain MA-11 was selected for its streamlined energy metabolism, faster aromatic conversion rates, and greater robustness to aromatics [21]. With the same process layout and feed regime, strain MA-11 achieved a final titer of 65 g L^{-1} MA within 80 h, which was similar to MA-1 (Fig. 4B). Notably, no byproducts, including gluconate or 2-ketogluconate, were secreted. Remarkably, the process reached a maximum volumetric productivity of 2 g L^{-1} h^{-1}; this

represented a 25 % increase compared with that of MA-1 (Table 3). Furthermore, owing to its superior growth stoichiometry, MA-11 required significantly less glucose, resulting in a higher overall carbon efficiency. The MA yield based on total carbon (0.58 mol mol^{-1}) was nearly 20 % greater than that of MA-1; these results demonstrated enhanced resource efficiency and reinforced the potential of genome reduction strategies for improving precision fermentation processes.

Taken together, these findings indicate that dynamic feeding strategies and genome reduction enhance the MA production efficiency. By integrating real-time adjustments based on cellular demand, the novel process concept enables a fully automated system, maintains optimal performance throughout the fermentation run and delivers MA at high yields with minimal byproducts. These findings highlight the potential of precision fermentation to address metabolic bottlenecks and enhance bioproduction from renewable substrates. Notably, the genome-reduced strain *P. putida* MA-11 not only achieved superior volumetric productivity and carbon efficiency but also demonstrated scalability for industrial applications. The enhanced performance of MA-11 may be attributed to specific advantages conferred by its streamlined genome, such as increased ATP availability and reduced maintenance demands [54]. These features likely supported processes like MA secretion—driven by proton symport and sensitive to the proton motive force —as well as stress defense mechanisms, explaining its superior performance in final process stages, observed here (Fig. 4) and before [21]. Additionally, the higher biomass yield of the genome-reduced chassis reduced the substrate requirement for cell growth [55].

Although direct intracellular measurements of ATP and NAD^+/NADH were not conducted, the consistent correlation between fermentation performance, flux redistribution, and energy-conserving adaptations supports the interpretation that glucose metabolism plays a central role in modulating energy supply and thereby influences MA production efficiency. Future studies involving targeted metabolite profiling are warranted to quantitatively validate this hypothesis and further refine energy-balanced process strategies.

3.8. Upscaling of the value chain enables fed-batch MA production from polystyrene-based crude benzoate

To evaluate the scalability of the polystyrene-based value chain, fed-batch fermentation was performed at a 100 mL scale using crude benzoate as the carbon source. A total of 5.75 g of crude benzoate (approximately 60 % benzoate content) was obtained from polystyrene photolysis and used to prepare a concentrated benzoate feed. *P. putida* MA-11 was selected for its favorable carbon and benzoate conversion efficiency (Table 3), and we applied the sophisticated dynamic control strategy to supply glucose and crude benzoate on demand. Over 42 h, the process proceeded smoothly, the final 5 mM dose of crude benzoate was fully converted, and a final titer of 21 g L^{-1} MA was attained (Fig. 5). However, over the following 6 h, no increase in the DO signal was observed; thus, crude benzoate conversion had stopped, indicating a depletion of metabolic capacity or inhibition. Despite these challenges, fermentation yielded approximately 600 mg of polystyrene-derived MA with a purity of 99.5 % after recovery and purification (Fig. S20).

Unlike its pure equivalent, the crude benzoate appeared to contain inhibitory components that imposed additional stress on the cells, leading to a stoppage in growth and efficient benzoate utilization. To accurately assess the composition of the starting material, we repeated the photolysis process using 20 g of polystyrene beads. This yielded 9.84 g of a light brown powder, which contained 67.3 % benzoate (Fig. S21), consistent with previous experiments. In this way, 6.3 g of benzoate was obtained from 20 g of PS beads, matching a yield of 31.6 %. NMR and GC/MS analyses identified benzoate and revealed that it was the predominant organic component, with only trace amounts of impurities detected (Fig. S21, Fig. S22, Fig. S23, Fig. S24). To identify inorganic side components, ion chromatography was conducted on an aqueous solution of the crude powder in deionized water, which had a slightly acidic pH of 3.56. The analysis revealed substantial amounts of sodium and chloride ions, suggesting the presence of residual salts from the neutralization and purification steps. Quantitative analysis showed that 1 g of the crude material contained approximately 0.67 g benzoate, 0.14 g sodium, and 0.17 g chloride, accounting for 97 % of the total mass.

Clearly, the fed-batch process using the crude benzoate feed was exposed to elevated salt levels, as the salt-rich feed had been alkalized by the addition of NaOH, introducing extra sodium ions into the system. To assess the impact of this increased salt load on microbial performance—given the known sensitivity of many microbes to high osmotic pressure [36]—we conducted growth experiments under controlled conditions. Sodium chloride (0–50 g L^{-1}) was added to a glucose medium supplemented with 5 mM benzoate and 20 g L^{-1} MA to simulate production conditions. The results showed that elevated salt concentrations strongly inhibited cell growth (Fig. 3E). Notably, strain MA-11 ceased growing entirely at 20 g L^{-1} NaCl. To remove the residual salt from the crude benzoate, a recrystallization step was implemented. This process yielded a white powder with a benzoate purity of 95.3 % (Fig. S21). Ion chromatography of an aqueous solution of the solid confirmed the effectiveness of the purification, detecting only trace amounts of sodium and chloride—each contributing less than 1 %. The mother liquor contained only 0.6 % benzoate. Subsequent sublimation enhanced the purity even further. HPLC, NMR and GC/MS analyses of both the recrystallized and sublimated fractions produced spectra that matched those of pure benzoic acid (Fig. S21, Fig. S22, Fig. S23, Fig. S24), confirming the absence of significant organic impurities.

Taken together, the optimized, still simple, purification workflow produced benzoate, effectively free of organic and inorganic contaminants. Given the high purity achieved, benzoate derived from polystyrene—after optimized purification— promises to approach the performance of pure commercial benzoate in the fermentation process, supporting equally efficient MA production.

3.9. Deletion of periplasmic glucose oxidation results in increased carbon efficiency for MA production at the expense of reduced stress tolerance

The accumulation of gluconate and 2-ketogluconate by *P. putida* MA-1 under stress suggested enhanced flux through the periplasmic glucose oxidation pathway (Fig. S11), a finding supported by metabolic flux analysis (Fig. 2). In contrast, both byproducts were absent under the

Table 3
Fed-batch performance parameters of *P. putida* MA producer strains MA-1, MA-11 and MA-12. Yields and productivities were calculated from two bioreactor replicates. All strains were exponentially fed with glucose and were given 5 mM shots of benzoate upon full conversion into MA triggered by an increase in in the DO signal. The maximum volumetric productivity (P_{Vmax}) and maximum specific productivity (P_{Smax}) correspond to the maximum volumetric and biomass-specific productivity, respectively (DCW, dry cell weight).

Strain	Genotype	Max. MA titer [g L^{-1}]	$Y_{MA/BA}$ [mol mol^{-1}]	$Y_{MA/Glc}$ [mol mol^{-1}]	$Y_{MA/(BA+Glc)}$ [mol mol^{-1}]	P_{Vmax} [g L^{-1} h^{-1}]	P_{Smax} [g g_{DCW}^{-1} h^{-1}]
MA-1	KT2440 *ΔcatBC*	64.9 ± 3.0	1.00 ± 0.04	0.96 ± 0.09	0.50 ± 0.02	1.56 ± 0.17	0.06 ± 0.01
MA-11	EM42 *ΔcatBC* P_{cat}:*catA2*	65.9 ± 3.5	1.00 ± 0.02	1.31 ± 0.05	0.58 ± 0.03	2.00 ± 0.20	0.09 ± 0.01
MA-12	KT2440 *ΔcatBC Δgcd*	53.3 ± 2.5	1.00 ± 0.02	1.66 ± 0.04	0.67 ± 0.03	1.74 ± 0.15	0.07 ± 0.01

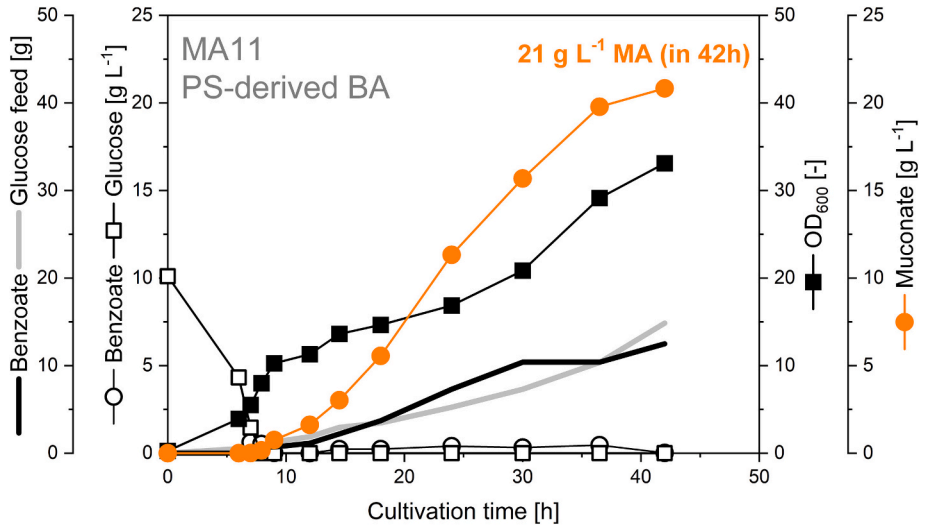

Fig. 5. Fed-batch production of MA from polystyrene-derived crude benzoate. The energy-optimized strain *P. putida* MA-11 was cultivated in glucose minimal medium with exponential feeding. The automatic addition of 5 mM benzoate pulses was synchronized with the increase in dissolved oxygen levels, indicating the complete conversion of the previous dose via benzoate and catechol dioxygenases.

precision fed-batch conditions, raising the question of whether—and to what extent—this periplasmic route still contributed when substrate availability was limited.

To investigate this, the periplasmic glucose oxidation pathway was disrupted. Therefore, the *gcd* gene encoding periplasmic glucose dehydrogenase was deleted in MA-1, yielding the *P. putida* MA-12 strain. Strain MA-12 grew slower (0.34 h^{-1}) than MA-1 but achieved a higher biomass yield without the secretion of gluconate or 2-ketogluconate in the presence of excess substrate, suggesting increased glucose metabolism efficiency [56]. Metabolic flux analysis confirmed that the glucose uptake was nearly entirely redirected to the cytosolic phosphorylation pathway (97 ± 4 %) (Fig. 2E); this doubled the fluxes through glucose-6-phosphate dehydrogenase (G6PDH) and increased the NADPH supply at the cost of increased ATP demand through the ATP-binding cassette (ABC) importer and the subsequent phosphorylation of glucose (Fig. 2F, Fig. S25). MA-12 exhibited significantly greater sensitivity to benzoate than MA-1 (Fig. S10F), suggesting that the periplasmic pathway, though dispensable under optimal growth conditions, plays a crucial role in stress defense.

In fed-batch experiments, MA-12 exhibited slower growth and needed more than 20 h to deplete the initial glucose (Fig. 4C). Upon DO-coupled benzoate feeding, MA production began but was stopped after reaching 20 g L^{-1}; this was accompanied by growth cessation and continued glucose accumulation due to reduced uptake. Glucose consumption was 20 % slower and 25 % lower than that of MA-1, resulting in a final MA titer of 50 g L^{-1}. Benzoate conversion slowed until it stopped entirely, preventing further substrate addition and stabilizing the titer.

While *P. putida* MA-12 initially maintained efficient glucose metabolism, its energy-generation capacity seemed insufficient over time to support sustained MA synthesis under increased production stress. This limitation, together with the increased sensitivity of MA-12 to high benzoate levels, highlights the role of periplasmic glucose metabolism in stress tolerance during high-level bioproduction. Nevertheless, strain MA-12 exhibited superior carbon efficiency and achieved a yield of 0.67 mol MA mol^{-1} (glucose plus benzoate); this value was 34 % higher than that of MA-1 and 15 % higher than that of MA-11 (Table 3).

The key conclusions regarding strain MA-12 are as follows: it performs efficiently under non-stress conditions and demonstrates improved glucose metabolism under glucose-excess conditions, effectively preventing the accumulation of gluconate and 2-ketogluconate. However, under production stress MA-12 showed low tolerance to benzoate (Fig. S10F) and diminished performance during the later stages of fed-batch cultivation (Fig. 4C), indicating that the periplasmic pathway is critical for stress defense. Consequently, MA-12 is not well-suited for high-level MA production in fed-batch processes. Nevertheless, it may hold promise as a chassis for future continuous production processes operating under lower-stress conditions, such as reduced MA titers and controlled benzoate feeding.

3.10. From MA to high-purity plastic monomers

To demonstrate downstream versatility, 400 mL of benzoate-free culture broth was subjected to downstream processing. MA was recovered by acidification (pH 1.3) and temperature reduction on ice, as described previously [18]. The purified MA crystals were filtered, washed with ultrapure water, and freeze-dried, yielding a product of 99 % purity. Fermentative MA was hydrogenated into adipic acid at a 10 g scale using ethanol or 2MTHF as green solvents, with a subsequent scale-up to 100 g using 2MTHF. This process produced 91 g of adipic acid (>98 % purity, ^{1}H NMR, ^{13}C NMR), with a yield of 88 % (Fig. S4, Fig. S5). The structure and melting point (151.9 °C) confirmed its alignment with known values (151–154 °C). Adipic acid was further reduced to hexanediol. A 10 g batch of commercial adipic acid yielded 51 % hexanediol, whereas 20 g of MA-derived adipic acid produced 7.6 g of hexanediol (>95 % purity, ^{1}H NMR, Fig. S6, Fig. S7), corresponding to a yield of 47 %. The melting point (39.8 °C) aligned with the reported range (38–42 °C). Finally, adipic acid was converted into hexamethylenediamine (HMDA). A 20 g batch was transformed into adipamide at 180 °C using urea under neat conditions, yielding 11.8 g (60 % yield, >90 % purity, ^{1}H NMR in DMSO-d_6; data not shown). A subsequent reduction of 10.5 g of adipamide yielded 2.1 g of HMDA after distillation (>98 % purity, ^{1}H NMR, Fig. S8). The product's melting point (40.2 °C) corresponded to known values (39–42 °C); these results confirmed successful conversion and product quality. These results also demonstrate the feasibility of converting fermentative benzoate-based MA into high-purity plastic monomers, supporting its potential for sustainable material synthesis.

3.11. Polymerization of adipic acid and hexamethylenediamine into PA66

Finally, we tested whether the fermentation-derived building blocks adipic acid and hexamethylenediamine could lead to the production of

polyamide-6,6 (PA66). The polymer was formed using a process similar to a typical industrial approach (Fig. S9), i.e., melt polymerization from a salt of the precursors [57]. A PA66 salt was synthesized by mixing ethanolic solutions of adipic acid and hexamethylenediamine, and both were derived from a novel value chain. For comparison, a PA66 salt was also prepared using commercial, crude oil-derived precursors. Both salts exhibited nearly identical pH values of 8.36–8.37 at 1 % *w*/w in water; this result was consistent with the slight excess of hexamethylenediamine, which imparted a mildly basic character. The melting point of both salts was 192 °C, which aligned with the reported values [58]. Prepolymers were produced by heating the salts in an autoclave under nitrogen. A subsequent polymerization step was performed in the solid state below the melting point of PA66 to yield the final polymer (Fig. 6A). The properties of the two polymers were analyzed for comparison. DSC revealed almost identical thermograms (Fig. S26, with T_m = 262 °C, T_c = 230–231 °C, and a crystallization enthalpy of 68 J g^{-1}, which corresponded to a crystallinity degree of 30 %. These results aligned with the values obtained by DSC for commercial PA66 [59]. SEC yielded almost identical chromatograms for fermentation-based and crude oil-based PA66 (Fig. S27), with corresponding $M_{n,SEC}$ values of 10.6 and 10.7 kDa, respectively, relative to the PMMA standards. Molar masses of >20 kDa rivalling industrial values could be attained by increasing the reaction time and removing water under vacuum [60]. In summary, the molar mass and thermal properties of the novel PA66 were virtually identical to those of petrochemical PA66; thus, fermentation-derived precursors could produce polymers with properties equivalent to those obtained from conventional petrochemical sources (Table 4, Fig. S28).

4. Discussion

4.1. Sustainability and market potential

The growing environmental impact of plastic waste needs innovative and scalable waste valorization solutions [61]. Polystyrene (PS) waste poses a significant challenge because of its long persistence in the environment and low recycling rates, which are driven primarily by high processing costs [62]. In this study, a novel cascaded approach to the upcycling of polystyrene (PS) waste into valuable chemical products, including MA, adipic acid, hexanediol, hexamethylenediamine, and nylon-6,6, is demonstrated using metabolically engineered *P. putida* KT2440 (Fig. 6A). Nylon-6,6 is a widely used synthetic polymer because of its durability, versatility, and performance in various industries, including textiles, automotive, and engineering plastics. However, its conventional production relies heavily on fossil-based resources and significantly contributes to carbon emissions [63]. The comparable mechanical and thermal properties of PS waste-based nylon-6,6 and its petrochemical counterpart confirm that this process meets industry standards (Table 4). Therefore, the approach may serve as a sustainable "drop-in" alternative for the nylon industry. This finding is crucial since it demonstrates that sustainable alternatives can seamlessly integrate into existing industrial supply chains as drop-in solutions to ensure compatibility with conventional manufacturing infrastructure [64]. The use of textile-based glucose as a growth substrate further enhances the process's sustainability, enabling the production of fully waste-based products. This dual waste stream approach highlights the versatility and broad applicability of the technology, facilitating future innovations in waste management and resource recovery [65]. Beyond the environmental benefits, the economic potential of this approach is substantial. Global polyamide production has reached 7 million tons annually, with applications spanning the automotive, electrical, textile, and medical sectors [66].The global market value of key nylon precursors highlights the financial viability of transitioning to waste-derived raw materials. Adipic acid is a key precursor for nylon-6,6 and has a global market value of approximately $6 billion annually [67]. Hexanediol is used in coatings and adhesives and is valued at approximately $2.5 billion. Hexamethylenediamine is another essential nylon precursor and has a market value of approximately $7.5 billion. By replacing fossil-based inputs with upcycled PS waste and textile waste, the proposed process aligns with circular economy principles, providing both environmental and economic incentives for industrial adoption. Moreover, recent advancements in the enzymatic degradation and recycling of polyamides have enabled monomer recovery, waste reduction, and circularity [68–70], aligning with this study's goal of fostering a sustainable, closed-loop plastic economy. Moreover, MA is gaining recognition as a high-value platform chemical because of its conjugated double bonds [71]; thus, it is a versatile monomer for the synthesis of specialty polymers, including polyester polyols, polyamides, and aromatic polyesters (Fig. 6B). The photolytic breakdown of polystyrene (PS), as applied in this study, has multiple advantages in terms of efficiency and sustainability, including low energy requirements, potentially using green energy, high selectivity [72], and direct fermentation of the crude photolysate without additional processing.

Toward a plastic waste biorefinery using polystyrene-derived input streams, future research should focus on further enhancing chemical depolymerization processes. The visible light-driven PS depolymerization provides a promising start point, given the fact that it is simple and selective, and operates under ambient temperature and pressure with cheap, readily available inorganic or organic acids as a simple catalysts [9]. It offers a more sustainable and efficient alternative for polystyrene breakdown compared to other reported photochemical methods, which rely on toxic transition metal catalysts, halogenated reagents, or organic solvents—factors that limit their scalability and environmental compatibility for plastic valorization [73–75].

Promising directions for increasing its efficiency include the use of flow photoreactor systems [76], supported by 3D-printed reactor technologies [77], and wavelength-tuned LEDs [78] to enable precise light distribution and controlled reaction times—factors that can significantly increase yields and improve process scalability [79]. The purification workflow was efficient and straightforward and appeared scalable, yielding benzoic acid at high purity (>97 %) and high recovery, with no detectable organic impurities. This was achieved using only simple extraction and washing steps applied to the crude photolysate. To enhance the sustainability of the process, future work could focus on replacing diethyl ether with greener solvent alternatives—such as ethyl acetate or 2-methyltetrahydrofuran—and exploring catalyst recycling strategies. In particular, *p*-toluenesulfonic acid could be recovered from the aqueous phase following benzoic acid removal via further acidification and crystallization.

Potential bottlenecks for scaling up the fed-batch fermentation include oxygen transfer limitations, due to the high oxygen demand of benzoate catabolism. Maintaining adequate DO levels at larger scale may require improved aeration and mixing. Precise glucose and benzoate feeding, crucial to the dynamic control strategy, may be harder to regulate due to slower sensor response and mixing delays. Additionally, metabolic stress from high MA or benzoate concentrations could intensify, especially with crude feedstocks that may contain inhibitors. While *P. putida* MA-11 improves robustness and carbon efficiency, its performance under industrial-scale stress remains to be validated. Finally, feedstock variability poses challenges that may require further purification or strain engineering. Addressing these scale-up bottlenecks will be essential to transition to robust, industrially viable production. To support this transition, future research should integrate life cycle assessment (LCA) and techno-economic analysis (TEA) to evaluate the environmental and economic performance of the full process chain. These tools will help identify sustainability hotspots, prioritize process improvements, and demonstrate the viability of polystyrene-to-nylon conversion as a competitive and circular alternative to fossil-based routes. Existing LCA and TEA studies on lignin aromatics-based [80] and plastic-based platform chemicals [81] might offer valuable methodological guidance and benchmarks that can inform future assessments of polystyrene-based value chains.

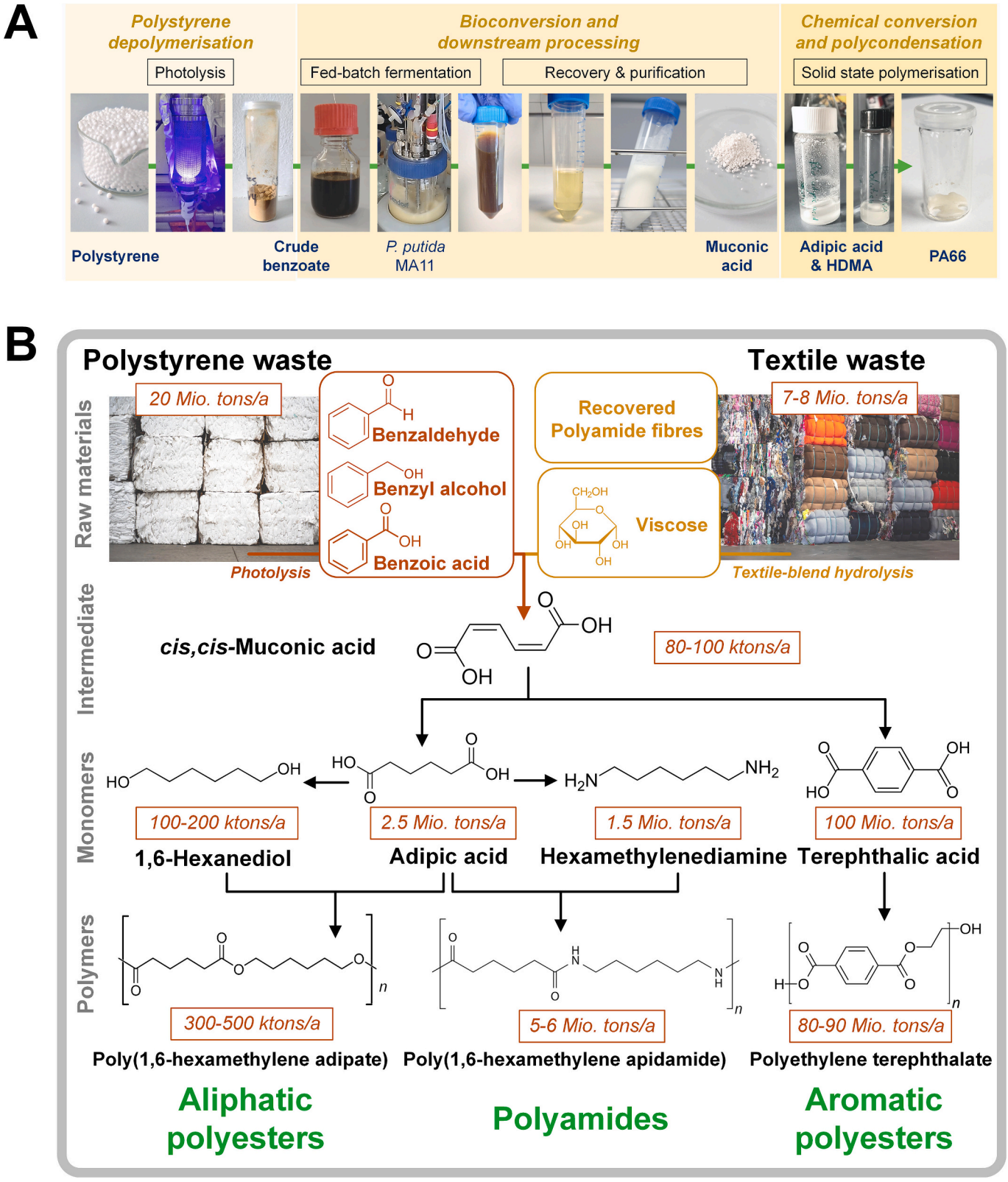

Fig. 6. Biological upcycling of polystyrene and textile waste into ready-to-use plastic monomers and polymers. Proof-of-concept demonstration of a polystyrene-to-nylon value chain encompassing cascaded chemical deconstruction, biological upcycling, chemical diversification, and final nylon polymerization (A). MA as a versatile platform building block for fully waste-based polyester polyols, polyamides, and aromatic polyesters (B). Polystyrene-waste image created by iStock.com/Dante Castillo; textile-waste image created by iStock.com/joruba.

Table 4
Molar mass and thermal properties of solid-phase polymerized PA66 produced from commercial adipic acid and hexamethylenediamine of petrochemical origin as well as fermentation-based monomers. The latter monomers were obtained from MA, which was upcycled from benzoate through a fermentative route using metabolically engineered *P. putida* MA-1. Molar mass characteristics were determined by SEC, and thermal analyses were performed by DSC.

Polymer properties	Upcycled PA66	Petrochemical PA66
$M_{n,SEC}$ (kg mol^{-1})[c]	10.6	10.7
$M_{w,SEC}$ (kg mol^{-1})[c]	44.2	48.3
$Đ$[c]	4.2	4.5
T_m (°C)[a]	262.3	261.7
T_c (°C)[a]	231.0	230.3
ΔH_c (J g^{-1})	68.1	68.0
Crystallinity (%)[b]	30.1	30.1

[a] The stated temperatures correspond to the peak maxima.
[b] The crystallinity was calculated as ΔH_c divided by the known value of 226 J g^{-1} for ΔH_m of 100 % crystalline PA66 [112].
[c] The value was assessed by SEC in hexafluoro isopropanol (HFiP) against PMMA standards.

While microbial depolymerization of polystyrene is an increasingly active research area, it currently suffers from major limitations: the process often requires weeks to months for observable weight loss, is typically confined to surface erosion, and lacks the efficiency needed for true bulk polymer degradation [82]. As such, it is not yet viable as a consolidated industrial solution. However, advanced microbial depolymerization, particularly when integrated with upstream chemical depolymerization, could represent a compelling next step [83]. Although the molecular weight of polystyrene decreased significantly during the photolytic depolymerization process used here, some oligomeric fragments of up to about 5–7 units remained after 7 days. Transforming these residual oligomers—alongside the monomers—through biological conversion within a hybrid chemical–biological recycling framework could enhance overall process performance, though it would require extensive enzyme engineering and metabolic optimization [84].

4.2. Insights into metabolic pathways under production conditions

A key finding of this study was that intracellular carbon fluxes in *P. putida* under stressful production conditions significantly deviated from those in normally growing cells and dynamically adapted throughout the process to counteract the progressively increasing stress caused by the accumulation of MA. Although *P. putida* is renowned for its resilience under industrial-scale stress conditions [85,86], prolonged exposure to inhibitory substrates and product concentrations leads to severe ATP and redox limitations (Fig. 2). As a result, the cells activate native escape mechanisms to mitigate the metabolic burden [87]. The conversion flux from benzoate to MA was drastically reduced (Fig. 2).

Transcriptomic and enzymatic analyses revealed that the observed downregulation of the benzoate degradation pathway under high stress was linked to repression of genes encoding benzoate transporters, putatively as a protective mechanism to limit further intracellular accumulation of the toxic substrate (Fig. 3). In contrast, genes encoding enzymes responsible for the downstream conversion and detoxification of benzoate into MA were upregulated, indicating a cellular strategy to process internalized benzoate efficiently while restricting additional influx. Genes of the *ben* operon are transcribed from different mRNAs, which could be a molecular basis for the observed decoupled expression. As a result, cells exposed to severe benzoate stress exhibited a 13-fold reduction in their ability to convert benzoate, as determined by in-vivo degradation assays (Fig. 3B). This finding closely mirrored the 11-fold decrease in pathway flux quantified by ^{13}C metabolic flux analysis (Fig. 2). Further research is needed to fully resolve this regulatory landscape [88]. Beyond transcriptional control, metabolite-level thermodynamic regulation has also been shown to influence fluxes in central carbon metabolism during the utilization of sugars and aromatics in *P. putida* [89] and related microbes [90]. These findings highlight the value of integrated multi-omics approaches for future investigations.

Clearly, benzoate acted as uncoupler of respiration and inhibitor of the electron transport chain [53,91]. The activation of periplasmic oxidation of glucose emerged as a central defense route against this stress. This flux change is a well-known, actively orchestrated survival

Table 5
Performance of benzoate-based MA production processes using metabolically engineered *P. putida*. The given MA titer corresponds to the highest reported value. P_V corresponds to the average space-time yield, calculated from the final titer divided by the process duration (*values estimated from reference assuming complete glucose conversion, n. a. – not accessible; B – Batch, FB – Fed-batch, pH – pH-based benzoate feeding, DO – dissolved oxygen-based benzoate feeding, EX – exponential feeding, AD – adaptive feeding, CO – benzoate–glucose cofeeding). The given circularity of a process concept refers to the raw materials used: • fossil benzoate, first-generation glucose; •• waste-based benzoate, first-generation glucose; ••• waste-based benzoate, waste-based glucose.

Strain	MA titer [g L^{-1}]	$P_{V, MA}$ [g L^{-1} h^{-1}]	$Y_{MA/(GLC+BA)}$ [mol mol^{-1}]	Mode	Benzoate feed pH | DO	Glucose feed	Circularity	Reference
MA-1				B	-	-	•	[18]
MA-1				B	-	-	••	This study
MA-1				B	-	-	•••	This study
CJ103*				B	-	-	•	[113][a]
BCM114*				B	-	-	•	[114][b]
JD1*				FB	● ○	EX	•	[30]
MA-11				FB	○ ●	AD	••	This study
BM014*			n.a.	FB	○ ●	CO	•	[115][c]
CJ102*			n.a.	FB	○ ●	CO	•	[17]
BN6*			n.a.	FB	● ○	EX	•	[80]
CJ242*			n.a.	FB	○ ●	CO	•	[19]
MA-12				FB	○ ●	AD	•	This study
MA-11				FB	○ ●	AD	•	This study
MA-1				FB	○ ●	AD	•	This study

[a] Vardon *et al.* [113], [b] Kim *et al.* [114], [c] Bang *et al.* [115].

strategy of *P. putida* to different types of stress [92,93]. Physiologically, this metabolic shift rapidly generates energy while depleting glucose, which is an easily degradable carbon source, and results in the accumulation of gluconate and 2-ketogluconate, which are less accessible to competing microbes [93]. From a bioprocessing perspective, periplasmic glucose oxidation appeared suboptimal since it diverted carbon away into byproducts and reduced the overall process efficiency. However, the genetic elimination of this pathway significantly impaired growth and overall performance, highlighting its critical role in maintaining the metabolic balance (Fig. 2, Fig. 4). The key to sustaining periplasmic oxidation while minimizing its drawbacks was to carefully regulate glucose availability through dynamic feeding, providing an optimal trade-off. By restricting glucose flux into the periplasm to a level that could be fully redirected into the cytosol for further breakdown, the process ensured efficient glucose metabolism without excessive carbon loss to byproducts (Fig. 4). To further improve redox and energy balances, future strategies might consider introducing the glucose facilitator Glf to replace the ATP-consuming ABC transporter, enabling passive glucose uptake and reducing energy demand [94]. Additionally, expressing NADPH-specific GapN would generate NADPH directly from glyceraldehyde-3-phosphate [95,96], supporting redox balance under production stress. Both interventions target key bottlenecks identified in the flux analysis and seem promising next steps for strain optimization.

In industrial fed-batch processes for chemical production, performance typically declines in the later stages as the product levels accumulate. For various engineered microbes [49,51,95,97–100], including *P. putida*-based cell factories [18,21] (Table 5), an initially high production rate during the early feed phase gradually decreases, leading to reduced product formation and metabolic activity over time. In many cases, elevated product concentrations, particularly organic acids [101], including MA [102], have been found to exert toxic effects on cells [95,97–99,103]. However, the underlying metabolic effects often remain unresolved, and processes are often empirically designed [104]. Based on these challenges, these processes should be analyzed in more detail at the flux level to identify the underlying metabolic challenges and limitations and to ultimately enable the design of superior strains and bioprocess strategies hand-in-hand.

As demonstrated, the precision fermentation strategy enhanced cellular metabolic capacity and enabled high MA titers by dynamically dosing glucose to limit growth while optimizing energy generation. This process allowed the production of up to 450 mM MA (Fig. 4), approaching the maximum tolerated concentration of 500 mM. Importantly, it mitigated key inhibitory effects of MA on glucose metabolism, particularly the shift toward low-energy glucose use and the secretion of gluconate and 2-ketogluconate (Fig. 2). However, the strategy did not fully overcome all possible inhibitory effects, such as disruption of the proton gradient. To address these limitations, additional efforts are required. Adaptive laboratory evolution may yield strains with enhanced MA tolerance [105], and cell recycling could support high-density cultures to offset reduced activity [106]. Alternatively, process designs such as in situ product removal or continuous fermentation could help maintain lower MA concentrations during production, albeit at the cost of increased process complexity.

4.3. Key advantages of the novel process

At the core of the developed value chain, the fed-batch fermentation process, which incorporates dynamically optimized glucose and benzoate feeding strategies, achieved a record-high MA titer of over 65 g L^{-1} from these substrates (Table 5). This represents the highest reported value to date and was accompanied by impressive volumetric productivities and carbon-based yields; these results highlighted the efficiency of the developed approach. Several critical design principles enabled the success of this process. Importantly, the selection of an optimal chassis strain—the engineered *P. putida* strains—demonstrated exceptional robustness and efficiency in converting PS-derived benzoate into MA. Notably, these strains tolerated benzoate and other PS-associated aromatics, such as benzaldehyde and benzyl alcohol, up to levels of 30 mM, supporting their suitability for applications where prolonged exposure to such substrates is common. Second, a striking advantage was the systems biology-guided fermentation process concept, which specifically keeps cells in an optimum metabolic state during production. The genome-reduced strain *P. putida* MA-11 and the periplasmic pathway mutant MA-12 were shown to be advantageous in enhancing process efficiency while reducing resource requirements. Their optimized metabolic performance improved the overall yield; thus, the process was economically viable and environmentally sustainable, even though strain MA-12 failed to reach the high MA titers of strains MA-1 and MA-11. While genome-reduced *P. putida* strains demonstrated advantages under the demanding fermentation conditions, such as MA-11 production (this study), catechol-based MA fed-batch production [21], and energy-intensive protein synthesis [32], other production scenarios showed no significant performance differences between the genome-reduced strains and their parental wild-type strains [107]. At first glance, this result could seem contradictory; however, the impact of genome reduction likely depended on the specific metabolic and environmental challenges encountered in each production setting. We concluded that the native robustness and metabolic versatility of *P. putida* enabled it to withstand many challenging production environments. Our ^{13}C metabolic flux data demonstrated that cells could effectively adapt to moderate stress conditions by dynamically readjusting pathway fluxes and adapting their energy and redox supplies (Fig. 2, Fig. S16, Fig. S17). However, under highly demanding conditions, such as nutrient limitation, prolonged exposure to toxic aromatic compounds, elevated product accumulation, and the physiological decline of aged cells after numerous doublings from the initial seed train, this adaptability could reach its limits. In these scenarios, genome reduction strategies could increase *P. putida* performance by eliminating unnecessary regulatory burdens, streamlining metabolic processes, and improving stress tolerance.

5. Conclusions

This study demonstrates an integrated framework for upcycling polystyrene waste into high-value chemicals and polymers through the combined use of metabolically engineered microorganisms and chemical synthesis. The conversion of PS-derived benzoate into muconic acid, followed by chemical transformation into nylon-6,6, establishes an effective microbial–chemical route for plastic waste valorization. These results confirm the feasibility of hybrid strategies for transforming polystyrene into industrially relevant products, complementing recent studies for plastic waste upcycling [108–110].

CRediT authorship contribution statement

Michael Kohlstedt: Writing – review & editing, Writing – original draft, Visualization, Validation, Software, Methodology, Investigation, Formal analysis, Data curation, Conceptualization. **Fabia Weiland:** Writing – review & editing, Visualization, Validation, Methodology, Investigation, Formal analysis. **Samuel Pearson:** Writing – review & editing, Validation, Methodology, Investigation, Formal analysis. **Devid Hero:** Writing – review & editing, Validation, Methodology, Investigation, Formal analysis. **Sophia Mihalyi:** Writing – review & editing, Validation, Methodology, Investigation, Formal analysis. **Laurenz Kramps:** Writing – review & editing, Validation, Methodology, Investigation, Formal analysis. **Georg Gübitz:** Writing – review & editing, Validation, Supervision, Resources, Funding acquisition, Formal analysis. **Markus Gallei:** Writing – review & editing, Validation, Supervision, Resources, Formal analysis. **Aránzazu del Campo:** Writing – review & editing, Validation, Supervision, Resources, Formal analysis. **Christoph Wittmann:** Writing – review & editing, Writing – original draft, Visualization, Validation, Supervision, Resources, Project

administration, Methodology, Funding acquisition, Formal analysis, Conceptualization.

Declaration of competing interest

The authors declare that they have no known competing financial interests or personal relationships that could have appeared to influence the work reported in this paper.

Acknowledgements

This project has received funding from the European Union's Horizon Europe Program under Grant Agreement number: 101057971. Christoph Wittmann acknowledges financial support from the German Ministry of Education and Research (BMBF) through grants Bio2Nylon (FKZ 03V0757) and LignoValue (FKZ 031B0344A). Fabia Weiland would like to thank the HaVo Foundation for funding her through a doctoral fellowship. Fabia Weiland and Michael Kohlstedt acknowledge support through a Young Investigator Award, sponsored by the Hans-and-Ruth-Giessen Foundation, St. Ingbert, Germany. The authors acknowledge the excellent assistance of Robert Drumm (INM) and David Kot (Fraunhofer Institute for Structural Durability and System Reliability, Division Plastics, Group Material Analytics, Darmstadt, Germany) for polymer analysis.

Appendix A. Supplementary data

Supplementary data to this article can be found online at https://doi.org/10.1016/j.cej.2025.168431.

Data availability

Data will be made available on request.

References

[1] V.M. Pathak, Navneet, Review on the current status of polymer degradation: a microbial approach, Bioresour. Bioprocess. 4 (1) (2017) 15, https://doi.org/10.1186/s40643-017-0145-9.
[2] J.R. Jambeck, R. Geyer, C. Wilcox, T.R. Siegler, M. Perryman, A. Andrady, R. Narayan, K.L. Law, Marine pollution. Plastic waste inputs from land into the ocean, Science 347 (6223) (2015) 768–771, https://doi.org/10.1126/science.1260352.
[3] Y. Zhang, J.N. Pedersen, B.E. Eser, Z. Guo, Biodegradation of polyethylene and polystyrene: from microbial deterioration to enzyme discovery, Biotechnol. Adv. 60 (2022) 107991, https://doi.org/10.1016/j.biotechadv.2022.107991.
[4] R.C. Thompson, C.J. Moore, F.S. vom Saal, S.H. Swan, Plastics, the environment and human health: current consensus and future trends, Philos. Trans. R. Soc. Lond. Ser. B Biol. Sci. 364 (1526) (2009) 2153–2166, https://doi.org/10.1098/rstb.2009.0053.
[5] Z. Peng, R. Chen, H. Li, Heterogeneous photocatalytic oxidative cleavage of polystyrene to aromatics at room temperature, ACS Sustain. Chem. Eng. 11 (29) (2023) 10688–10697, https://doi.org/10.1021/acssuschemeng.3c01282.
[6] N.F. Nikitas, E. Skolia, P.L. Gkizis, I. Triandafillidi, C.G. Kokotos, Photochemical aerobic upcycling of polystyrene plastics to commodity chemicals using anthraquinone as the photocatalyst, Green Chem. 25 (12) (2023) 4750–4759, https://doi.org/10.1039/D3GC00986F.
[7] Y. Qin, T. Zhang, H.Y.V. Ching, G.S. Raman, S. Das, Integrated strategy for the synthesis of aromatic building blocks via upcycling of real-life plastic wastes, Chem 8 (9) (2022) 2472–2484, https://doi.org/10.1016/j.chempr.2022.06.002.
[8] S. Oh, E.E. Stache, Chemical upcycling of commercial polystyrene via catalyst-controlled photooxidation, J. Am. Chem. Soc. 144 (13) (2022) 5745–5749, https://doi.org/10.1021/jacs.2c01411.
[9] Z. Huang, M. Shanmugam, Z. Liu, A. Brookfield, E.L. Bennett, R. Guan, D.E. Vega Herrera, J.A. Lopez-Sanchez, A.G. Slater, E.J.L. McInnes, X. Qi, J. Xiao, Chemical recycling of polystyrene to valuable xhemicals via selective acid-catalyzed aerobic oxidation under visible light, J. Am. Chem. Soc. 144 (14) (2022) 6532–6542, https://doi.org/10.1021/jacs.2c01410.
[10] R. Cao, M.-Q. Zhang, C. Hu, D. Xiao, M. Wang, D. Ma, Catalytic oxidation of polystyrene to aromatic oxygenates over a graphitic carbon nitride catalyst, Nat. Commun. 13 (1) (2022) 4809, https://doi.org/10.1038/s41467-022-32510-x.
[11] E. Belda, R.G.A. van Heck, M.J. Lopez-Sanchez, S. Cruveiller, V. Barbe, C. Fraser, H.P. Klenk, J. Petersen, A. Morgat, P.I. Nikel, D. Vallenet, Z. Rouy, A. Sekowska, V.A.P.M. dos Santos, V. de Lorenzo, A. Danchin, C. Medigue, The revisited genome of *Pseudomonas putida* KT2440 enlightens its value as a robust metabolic chassis, Environ. Microbiol. 18 (10) (2016) 3403–3424, https://doi.org/10.1111/1462-2920.13230.
[12] J.I. Jiménez, B. Miñambres, J.L. García, E. Díaz, Genomic analysis of the aromatic catabolic pathways from *Pseudomonas putida* KT2440, Environ. Microbiol. 4 (12) (2002) 824–841, https://doi.org/10.1046/j.1462-2920.2002.00370.x.
[13] Y.H. Kim, K. Cho, S.H. Yun, J.Y. Kim, K.H. Kwon, J.S. Yoo, S.I. Kim, Analysis of aromatic catabolic pathways in *Pseudomonas putida* KT 2440 using a combined proteomic approach: 2-DE/MS and cleavable isotope-coded affinity tag analysis, Proteomics 6 (4) (2006) 1301–1318, https://doi.org/10.1002/pmic.200500329.
[14] P.I. Nikel, M. Chavarría, A. Danchin, V. de Lorenzo, From dirt to industrial applications: *Pseudomonas putida* as a synthetic biology chassis for hosting harsh biochemical reactions, Curr. Opin. Chem. Biol. 34 (2016) 20–29, https://doi.org/10.1016/j.cbpa.2016.05.011.
[15] J. Nogales, J.L. García, E. Díaz, Degradation of aromatic compounds in *Pseudomonas*: A systems biology view, in: F. Rojo (Ed.), Aerobic Utilization of Hydrocarbons, Oils and Lipids, Springer International Publishing, Cham, 2017, pp. 1–49, https://doi.org/10.1007/978-3-319-39782-5_32-1.
[16] A. Weimer, M. Kohlstedt, D.C. Volke, P.I. Nikel, C. Wittmann, Industrial biotechnology of *Pseudomonas putida*: advances and prospects, Appl. Microbiol. Biotechnol. 104 (18) (2020) 7745–7766, https://doi.org/10.1007/s00253-020-10811-9.
[17] D.R. Vardon, N.A. Rorrer, D. Salvachua, A.E. Settle, C.W. Johnson, M.J. Menart, N.S. Cleveland, P.N. Ciesielski, K.X. Steirer, J.R. Dorgan, G.T. Beckham, *cis,cis*-Muconic acid: separation and catalysis to bio-adipic acid for nylon-6,6 polymerization, Green Chem. 18 (11) (2016) 3397–3413, https://doi.org/10.1039/C5GC02844B.
[18] M. Kohlstedt, S. Starck, N. Barton, J. Stolzenberger, M. Selzer, K. Mehlmann, R. Schneider, D. Pleissner, J. Rinkel, J.S. Dickschat, J. Venus, B.J.H. v.D. J, C. Wittmann, From lignin to nylon: cascaded chemical and biochemical conversion using metabolically engineered *Pseudomonas putida*, Metab. Eng. 47 (2018) 279–293, https://doi.org/10.1016/j.ymben.2018.03.003.
[19] D. Salvachua, C.W. Johnson, C.A. Singer, H. Rohrer, D.J. Peterson, B.A. Black, A. Knapp, G.T. Beckham, Bioprocess development for muconic acid production from aromatic compounds and lignin, Green Chem. 20 (21) (2018) 5007–5019, https://doi.org/10.1039/c8gc02519c.
[20] H. Almqvist, H. Veras, K.N. Li, J.G. Hidalgo, C. Hulteberg, M. Gorwa-Grauslund, N.S. Parachin, M. Carlquist, Muconic acid production using engineered *Pseudomonas putida* KT2440 and a guaiacol-rich fraction derived from Kraft lignin, ACS Sustain. Chem. Eng. 9 (24) (2021) 8097–8106, https://doi.org/10.1021/acssuschemeng.1c00933.
[21] M. Kohlstedt, A. Weimer, F. Weiland, J. Stolzenberger, M. Selzer, M. Sanz, L. Kramps, C. Wittmann, Biobased PET from lignin using an engineered cis, cis-muconate-producing *Pseudomonas putida* strain with superior robustness, energy and redox properties, Metab. Eng. 72 (2022) 337–352, https://doi.org/10.1016/j.ymben.2022.05.001.
[22] J.M. Borrero-de Acuna, I. Gutierrez-Urrutia, C. Hidalgo-Dumont, C. Aravena-Carrasco, M. Orellana-Saez, N. Palominos-Gonzalez, J. van Duuren, V. Wagner, L. Glaser, J. Becker, M. Kohlstedt, F.C. Zacconi, C. Wittmann, I. Poblete-Castro, Channelling carbon flux through the meta-cleavage route for improved poly(3-hydroxyalkanoate) production from benzoate and lignin-based aromatics in *Pseudomonas putida* H, Microb. Biotechnol. 14 (6) (2021) 2385–2402, https://doi.org/10.1111/1751-7915.13705.
[23] P. Dvořák, P.I. Nikel, J. Damborský, V. de Lorenzo, Bioremediation 3.0: engineering pollutant-removing bacteria in the times of systemic biology, Biotechnol. Adv. 35 (7) (2017) 845–866, https://doi.org/10.1016/j.biotechadv.2017.08.001.
[24] C.W. Johnson, G.T. Beckham, Aromatic catabolic pathway selection for optimal production of pyruvate and lactate from lignin, Metab. Eng. 28 (2015) 240–247, https://doi.org/10.1016/j.ymben.2015.01.005.
[25] A.Z. Werner, W.T. Cordell, C.W. Lahive, B.C. Klein, C.A. Singer, E.C.D. Tan, M. A. Ingraham, K.J. Ramirez, D.H. Kim, J.N. Pedersen, C.W. Johnson, B.F. Pfleger, G.T. Beckham, D. Salvachúa, Lignin conversion to β-ketoadipic acid by *Pseudomonas putida* via metabolic engineering and bioprocess development, Sci. Adv. 9 (36) (2023) eadj0053, https://doi.org/10.1126/sciadv.adj0053.
[26] M. Kohlstedt, S. Starck, N. Barton, J. Stolzenberger, M. Selzer, K. Mehlmann, R. Schneider, D. Pleissner, J. Rinkel, J.S. Dickschat, J. Venus, J.B.J.H. van Duuren, C. Wittmann, From lignin to nylon: cascaded chemical and biochemical conversion using metabolically engineered *Pseudomonas putida*, Metab. Eng. 47 (2018) 279–293, https://doi.org/10.1016/j.ymben.2018.03.003.
[27] E. Martínez-García, V. de Lorenzo, Engineering multiple genomic deletions in gram-negative bacteria: analysis of the multi-resistant antibiotic profile of *Pseudomonas putida* KT2440, Environ. Microbiol. 13 (10) (2011) 2702–2716.
[28] I. Poblete-Castro, D. Binger, A. Rodrigues, J. Becker, V.A. Martins Dos Santos, C. Wittmann, In-silico-driven metabolic engineering of *Pseudomonas putida* for enhanced production of poly-hydroxyalkanoates, Metab. Eng. 15 (2013) 113–123, https://doi.org/10.1016/j.ymben.2012.10.004.
[29] M. Kohlstedt, C. Wittmann, GC-MS-based C-13 metabolic flux analysis resolves the parallel and cyclic glucose metabolism of *Pseudomonas putida* KT2440 and *Pseudomonas aeruginosa* PAO1, Metab. Eng. 54 (2019) 35–53, https://doi.org/10.1016/j.ymben.2019.01.008.
[30] J.B. van Duuren, D. Wijte, B. Karge, V.A. dos Santos, Y. Yang, A.E. Mars, G. Eggink, pH-stat fed-batch process to enhance the production of *cis, cis*-muconate from benzoate by *Pseudomonas putida* KT2440-JD1, Biotechnol. Prog. 28 (1) (2012) 85–92, https://doi.org/10.1002/btpr.709.

[31] C. Wittmann, A.P. Zeng, W.D. Deckwer, Growth inhibition by ammonia and use of a pH-controlled feeding strategy for the effective cultivation of *Mycobacterium chlorophenolicum*, Appl. Microbiol. Biotechnol. 44 (3–4) (1995) 519–525.
[32] S. Lieder, P.I. Nikel, V. de Lorenzo, R. Takors, Genome reduction boosts heterologous gene expression in *Pseudomonas putida*, Microb. Cell Factories 14 (2015) 23, https://doi.org/10.1186/s12934-015-0207-7.
[33] F. Weiland, N. Barton, M. Kohlstedt, J. Becker, C. Wittmann, Systems metabolic engineering upgrades *Corynebacterium glutamicum* to high-efficiency *cis*, *cis*-muconic acid production from lignin-based aromatics, Metab. Eng. 75 (2023) 153–169, https://doi.org/10.1016/j.ymben.2022.12.005.
[34] J.I. Jiménez, D. Pérez-Pantoja, M. Chavarría, E. Díaz, V. de Lorenzo, A second chromosomal copy of the catA gene endows Pseudomonas putida mt-2 with an enzymatic safety valve for excess of catechol, Environ. Microbiol. 16 (6) (2014) 1767–1778, https://doi.org/10.1111/1462-2920.12361.
[35] C. Wittmann, Fluxome analysis using GC-MS, Microb. Cell Factories 6 (2007) 6, https://doi.org/10.1186/1475-2859-6-6.
[36] M. Kohlstedt, P.K. Sappa, H. Meyer, S. Maass, A. Zaprasis, T. Hoffmann, J. Becker, L. Steil, M. Hecker, J.M. van Dijl, M. Lalk, U. Mader, J. Stulke, E. Bremer, U. Volker, C. Wittmann, Adaptation of *Bacillus subtilis* carbon core metabolism to simultaneous nutrient limitation and osmotic challenge: a multi-omics perspective, Environ. Microbiol. 16 (6) (2014) 1898–1917, https://doi.org/10.1111/1462-2920.12438.
[37] J.B.J.H. van Duuren, J. Puchałka, A.E. Mars, R. Bücker, G. Eggink, C. Wittmann, V.A.P.M. dos Santos, Reconciling in vivo and in silico key biological parameters of *Pseudomonas putida* KT2440 during growth on glucose under carbon-limited condition, BMC Biotechnol. 13 (1) (2013) 93, https://doi.org/10.1186/1472-6750-13-93.
[38] L.E. Quek, C. Wittmann, L.K. Nielsen, J.O. Krömer, OpenFLUX: efficient modelling software for ^{13}C-based metabolic flux analysis, Microb. Cell Factories 8 (2009) 25, https://doi.org/10.1186/1475-2859-8-25.
[39] W.A. van Winden, C. Wittmann, E. Heinzle, J.J. Heijnen, Correcting mass isotopomer distributions for naturally occurring isotopes, Biotechnol. Bioeng. 80 (4) (2002) 477–479, https://doi.org/10.1002/bit.10393.
[40] C. Wittmann, E. Heinzle, Genealogy profiling through strain improvement by using metabolic network analysis: metabolic flux genealogy of several generations of lysine-producing corynebacteria, Appl. Environ. Microbiol. 68 (12) (2002) 5843–5859.
[41] Y. Sasanuma, T. Ono, Y. Kuroda, E. Miyazaki, K. Hikino, J. Arou, K. Nakata, H. Inaba, K.-i. Tozaki, H. Hayashi, K. Yamaguchi, Structure−property correlations in model compounds of oligomer liquid crystals, J. Phys. Chem. B 108 (35) (2004) 13163–13176, https://doi.org/10.1021/jp040135h.
[42] D.A.G. Francis, R.E. Emmet, Preparation of amides, 1938.
[43] T. Li, A. Vijeta, C. Casadevall, A.S. Gentleman, T. Euser, E. Reisner, Bridging plastic recycling and organic catalysis: photocatalytic deconstruction of polystyrene via a C–H oxidation pathway, ACS Catal. 12 (14) (2022) 8155–8163, https://doi.org/10.1021/acscatal.2c02292.
[44] R. Shrivastava, A. Basu, P.S. Phale, Purification and characterization of benzyl alcohol- and benzaldehyde- dehydrogenase from *Pseudomonas putida* CSV86, Arch. Microbiol. 193 (8) (2011) 553–563, https://doi.org/10.1007/s00203-011-0697-6.
[45] S.M. Gritsch, S. Mihalyi, A. Bartl, W. Ipsmiller, U. Jenull-Halver, R.F. Putz, F. Quartinello, G.M. Guebitz, Closing the cycle: enzymatic recovery of high purity glucose and polyester from textile blends, Resour. Conserv. Recycl. 188 (2023) 106701, https://doi.org/10.1016/j.resconrec.2022.106701.
[46] S.M. Gritsch, S. Mihalyi, A. Bartl, W. Ipsmiller, U. Jenull-Halver, R.F. Putz, F. Quartinello, G.M. Guebitz, Closing the cycle: enzymatic recovery of high purity glucose and polyester from textile blends, Resour. Conserv. Recycl. 188 (2023) 106701, https://doi.org/10.1016/j.resconrec.2022.106701.
[47] S. Mihalyi, E. Sykacek, C. Campano, N. Hernández-Herreros, A. Rodríguez, A. Mautner, M.A. Prieto, F. Quartinello, G.M. Guebitz, Bio-upcycling of viscose/polyamide textile blends waste to biopolymers and fibers, Resour. Conserv. Recycl. 208 (2024) 107712, https://doi.org/10.1016/j.resconrec.2024.107712.
[48] C. Wittmann, J. Weber, E. Betiku, J. Krömer, D. Bohm, U. Rinas, Response of fluxome and metabolome to temperature-induced recombinant protein synthesis in *Escherichia coli*, J. Biotechnol. 132 (4) (2007) 375–384, https://doi.org/10.1016/j.jbiotec.2007.07.495.
[49] J. Becker, O. Zelder, S. Haefner, H. Schröder, C. Wittmann, From zero to hero-design-based systems metabolic engineering of *Corynebacterium glutamicum* for l-lysine production, Metab. Eng. 13 (2) (2011) 159–168, https://doi.org/10.1016/j.ymben.2011.01.003.
[50] H. Driouch, G. Melzer, C. Wittmann, Integration of *in vivo* and *in silico* metabolic fluxes for improvement of recombinant protein production, Metab. Eng. 14 (1) (2012) 47–58, https://doi.org/10.1016/j.ymben.2011.11.002.
[51] S.L. Hoffmann, L. Jungmann, S. Schiefelbein, L. Peyriga, E. Cahoreau, J. C. Portais, J. Becker, C. Wittmann, Lysine production from the sugar alcohol mannitol: design of the cell factory *Corynebacterium glutamicum* SEA-3 through integrated analysis and engineering of metabolic pathway fluxes, Metab. Eng. 47 (2018) 475–487, https://doi.org/10.1016/j.ymben.2018.04.019.
[52] S.K. Schwechheimer, J. Becker, L. Peyriga, J.C. Portais, C. Wittmann, Metabolic flux analysis in *Ashbya gossypii* using (13)C-labeled yeast extract: industrial riboflavin production under complex nutrient conditions, Microb. Cell Factories 17 (1) (2018) 162, https://doi.org/10.1186/s12934-018-1003-y.
[53] P.H. Lou, B.S. Hansen, P.H. Olsen, S. Tullin, M.P. Murphy, M.D. Brand, Mitochondrial uncouplers with an extraordinary dynamic range, Biochem. J. 407 (1) (2007) 129–140, https://doi.org/10.1042/bj20070606.
[54] E. Martínez-García, V. de Lorenzo, *Pseudomonas putida* as a synthetic biology chassis and a metabolic engineering platform, Curr. Opin. Biotechnol. 85 (2024) 103025, https://doi.org/10.1016/j.copbio.2023.103025.
[55] E. Martinez-Garcia, P.I. Nikel, T. Aparicio, V. de Lorenzo, *Pseudomonas* 2.0: genetic upgrading of *P. putida* KT2440 as an enhanced host for heterologous gene expression, Microb. Cell Factories 13 (2014) 159, https://doi.org/10.1186/s12934-014-0159-3.
[56] G.J. Bentley, N. Narayanan, R.K. Jha, D. Salvachúa, J.R. Elmore, G.L. Peabody, B. A. Black, K. Ramirez, A. De Capite, W.E. Michener, Engineering glucose metabolism for enhanced muconic acid production in *Pseudomonas putida* KT2440, Metab. Eng. 59 (2020) 64–75.
[57] R.J. Gaymans, Polyamides, in: M.E. Rogers, T.E. Long (Eds.), Synthetic Methods in Step-growth Polymers, John Wiley & Sons, Inc, 2003, pp. 135–195.
[58] C.D. Papaspyrides, Solid state polyamidation of aliphatic diamine-aliphatic diacid salts: a generalized mechanism for the effect of polycondensation water on reaction behaviour, Polymer 31 (3) (1990) 490–495, https://doi.org/10.1016/0032-3861(90)90391-B.
[59] A.M. Rhoades, J.L. Williams, R. Androsch, Crystallization kinetics of polyamide 66 at processing-relevant cooling conditions and high supercooling, Thermochim. Acta 603 (2015) 103–109, https://doi.org/10.1016/j.tca.2014.10.020.
[60] E. Roerdink, J.M.M. Warnier, Preparation and properties of high molar mass nylon-4,6: a new development in nylon polymers, Polymer 26 (10) (1985) 1582–1588, https://doi.org/10.1016/0032-3861(85)90098-9.
[61] Z. Xu, D. Sun, J. Xu, R. Yang, J.D. Russell, G. Liu, Progress and challenges in polystyrene recycling and upcycling, ChemSusChem 17 (17) (2024) e202400474, https://doi.org/10.1002/cssc.202400474.
[62] N. Chaukura, W. Gwenzi, T. Bunhu, D.T. Ruziwa, I. Pumure, Potential uses and value-added products derived from waste polystyrene in developing countries: a review, Resour. Conserv. Recycl. 107 (2016) 157–165, https://doi.org/10.1016/j.resconrec.2015.10.031.
[63] J. Zheng, S. Suh, Strategies to reduce the global carbon footprint of plastics, Nat. Clim. Chang. 9 (5) (2019) 374–378, https://doi.org/10.1038/s41558-019-0459-z.
[64] J.-G. Rosenboom, R. Langer, G. Traverso, Bioplastics for a circular economy, Nat. Rev. Mater. 7 (2) (2022) 117–137, https://doi.org/10.1038/s41578-021-00407-8.
[65] H.Y. Leong, C.-K. Chang, K.S. Khoo, K.W. Chew, S.R. Chia, J.W. Lim, J.-S. Chang, P.L. Show, Waste biorefinery towards a sustainable circular bioeconomy: a solution to global issues, Biotechnol. Biofuels 14 (1) (2021) 87, https://doi.org/10.1186/s13068-021-01939-5.
[66] J.A. Lee, J.Y. Kim, J.H. Ahn, Y.-J. Ahn, S.Y. Lee, Current advancements in the bio-based production of polyamides, Trends Chem 5 (12) (2023) 873–891, https://doi.org/10.1016/j.trechm.2023.10.001.
[67] J.W. Lee, H.U. Kim, S. Choi, J. Yi, S.Y. Lee, Microbial production of building block chemicals and polymers, Curr. Opin. Biotechnol. 22 (6) (2011) 758–767, https://doi.org/10.1016/j.copbio.2011.02.011.
[68] J. de Witt, T. Luthe, J. Wiechert, K. Jensen, T. Polen, A. Wirtz, S. Thies, J. Frunzke, B. Wynands, N. Wierckx, Upcycling of polyamides through chemical hydrolysis and engineered *Pseudomonas putida*, Nat. Microbiol. 10 (3) (2025) 667–680, https://doi.org/10.1038/s41564-025-01929-5.
[69] J. de Witt, M.-E. Ostheller, K. Jensen, C.A.M.R. van Slagmaat, T. Polen, G. Seide, S. Thies, B. Wynands, N. Wierckx, Increasing the diversity of nylonases for poly (ester amide) degradation, Green Chem. 26 (18) (2024) 9911–9922, https://doi.org/10.1039/D4GC01662A.
[70] R. Wei, G. Weber, L.M. Blank, U.T. Bornscheuer, Process insights for harnessing biotechnology for plastic depolymerization, Nat. Chem. Eng. 2 (2) (2025) 110–117, https://doi.org/10.1038/s44286-024-00171-w.
[71] I. Khalil, G. Quintens, T. Junkers, M. Dusselier, Muconic acid isomers as platform chemicals and monomers in the biobased economy, Green Chem. 22 (5) (2020) 1517–1541, https://doi.org/10.1039/C9GC04161C.
[72] S. Jiang, Y. Chen, Y. Huang, P. Hu, Photooxidation of polystyrene into high-value chemicals, Eur. J. Org. Chem. 28 (4) (2025) e202401109, https://doi.org/10.1002/ejoc.202401109.
[73] N.F. Nikitas, E. Skolia, P.L. Gkizis, I. Triandafillidi, C.G. Kokotos, Photochemical aerobic upcycling of polystyrene plastics to commodity chemicals using anthraquinone as the photocatalyst, Green Chem. 25 (12) (2023) 4750–4759, https://doi.org/10.1039/D3GC00986F.
[74] O.G. Mountanea, E. Skolia, C.G. Kokotos, Photochemical aerobic upcycling of polystyrene plastics via synergistic indirect HAT catalysis, Chem. Eur. J. 30 (44) (2024) e202401588, https://doi.org/10.1002/chem.202401588.
[75] E. Xu, T. Liu, F. Xie, J. He, Y. Zhang, Aerobic oxidation of alkylarenes and polystyrene waste to benzoic acids via a copper-based catalyst, Chem. Sci. 16 (4) (2025) 2004–2014, https://doi.org/10.1039/D4SC03269A.
[76] M. Zhang, P. Roth, Flow photochemistry — from microreactors to large-scale processing, Curr. Opin. Chem. Eng. 39 (2023) 100897, https://doi.org/10.1016/j.coche.2023.100897.
[77] E.G. Gordeev, K.S. Erokhin, A.D. Kobelev, J.V. Burykina, P.V. Novikov, V. P. Ananikov, Exploring metallic and plastic 3D printed photochemical reactors for customizing chemical synthesis, Sci. Rep. 12 (1) (2022) 3780, https://doi.org/10.1038/s41598-022-07583-9.
[78] J.P. Menzel, B.B. Noble, J.P. Blinco, C. Barner-Kowollik, Predicting wavelength-dependent photochemical reactivity and selectivity, Nat. Commun. 12 (1) (2021) 1691, https://doi.org/10.1038/s41467-021-21797-x.
[79] F. Lévesque, M.J. Di Maso, K. Narsimhan, M.K. Wismer, J.R. Naber, Design of a kilogram scale, plug flow photoreactor enabled by high power LEDs, Org. Process.

Res. Dev. 24 (12) (2020) 2935–2940, https://doi.org/10.1021/acs.oprd.0c00373.
[80] J.B.J.H. van Duuren, P.J. de Wild, S. Starck, C. Bradtmöller, M. Selzer, K. Mehlmann, R. Schneider, M. Kohlstedt, I. Poblete-Castro, J. Stolzenberger, N. Barton, M. Fritz, S. Scholl, J. Venus, C. Wittmann, Limited life cycle and cost assessment for the bioconversion of lignin-derived aromatics into adipic acid, Biotech. Bioeng. 17 (2020) 1381–1393.
[81] R.E. Vera, K.A. Vivas, N. Forfora, R. Marquez, I. Urdaneta, R. Frazier, C. Abbati de Assis, T. de Assis, T. Treasure, M. Farrell, M. Ankeny, D. Saloni, L. Pal, H. Jameel, R. Gonzalez, From waste to advanced resource: techno-economic and life cycle assessment behind the integration of polyester recycling and glucose production to valorize fast fashion garments, Chem. Eng. J. 500 (2024) 156895, https://doi.org/10.1016/j.cej.2024.156895.
[82] S. Ghatge, Y. Yang, J.-H. Ahn, H.-G. Hur, Biodegradation of polyethylene: a brief review, Appl. Biol. Chem. 63 (1) (2020) 27, https://doi.org/10.1186/s13765-020-00511-3.
[83] Y. Zhang, J.N. Pedersen, B.E. Eser, Z. Guo, Biodegradation of polyethylene and polystyrene: from microbial deterioration to enzyme discovery, Biotechnol. Adv. 60 (2022) 107991, https://doi.org/10.1016/j.biotechadv.2022.107991.
[84] N. Mohanan, Z. Montazer, P.K. Sharma, D.B. Levin, Microbial and enzymatic degradation of synthetic plastics, Front. Microbiol. 11 (2020) (2020), https://doi.org/10.3389/fmicb.2020.580709.
[85] A. Ankenbauer, R.A. Schäfer, S.C. Viegas, V. Pobre, B. Voß, C.M. Arraiano, R. Takors, *Pseudomonas putida* KT2440 is naturally endowed to withstand industrial-scale stress conditions, Microb. Biotechnol. 13 (4) (2020) 1145–1161, https://doi.org/10.1111/1751-7915.13571.
[86] P. Demling, A. Ankenbauer, B. Klein, S. Noack, T. Tiso, R. Takors, L.M. Blank, *Pseudomonas putida* KT2440 endures temporary oxygen limitations, Biotechnol. Bioeng. 118 (12) (2021) 4735–4750, https://doi.org/10.1002/bit.27938.
[87] P.I. Nikel, T. Fuhrer, M. Chavarria, A. Sanchez-Pascuala, U. Sauer, V. de Lorenzo, Reconfiguration of metabolic fluxes in *Pseudomonas putida* as a response to sub-lethal oxidative stress, ISME J. 15 (6) (2021) 1751–1766, https://doi.org/10.1038/s41396-020-00884-9.
[88] M.A. Kukurugya, C.M. Mendonca, M. Solhtalab, R.A. Wilkes, T.W. Thannhauser, L. Aristilde, Multi-omics analysis unravels a segregated metabolic flux network that tunes co-utilization of sugar and aromatic carbons in *Pseudomonas putida*, J. Biol. Chem. 294 (21) (2019) 8464–8479, https://doi.org/10.1074/jbc.RA119.007885.
[89] S. Sudarsan, L.M. Blank, A. Dietrich, O. Vielhauer, R. Takors, A. Schmid, M. Reuss, Dynamics of benzoate metabolism in *Pseudomonas putida* KT2440, Metab Eng Commun 3 (2016) 97–110, https://doi.org/10.1016/j.meteno.2016.03.005.
[90] R.A. Wilkes, J. Waldbauer, A. Carroll, M. Nieto-Domínguez, D.J. Parker, L. Zhang, A.M. Guss, L. Aristilde, Complex regulation in a Comamonas platform for diverse aromatic carbon metabolism, Nat. Chem. Biol. 19 (5) (2023) 651–662, https://doi.org/10.1038/s41589-022-01237-7.
[91] C. Norman, K.A. Howell, A.H. Millar, J.M. Whelan, D.A. Day, Salicylic acid is an uncoupler and inhibitor of mitochondrial electron transport, Plant Physiol. 134 (1) (2004) 492–501, https://doi.org/10.1104/pp.103.031039.
[92] D.C. Volke, N. Gurdo, R. Milanesi, P.I. Nikel, Time-resolved, deuterium-based fluxomics uncovers the hierarchy and dynamics of sugar processing by *Pseudomonas putida*, Metab. Eng. 79 (2023) 159–172, https://doi.org/10.1016/j.ymben.2023.07.004.
[93] A. Weimer, L. Pause, F. Ries, M. Kohlstedt, L. Adrian, J. Kromer, B. Lai, C. Wittmann, Systems biology of electrogenic Pseudomonas putida - multi-omics insights and metabolic engineering for enhanced 2-ketogluconate production, Microb. Cell Factories 23 (1) (2024) 246, https://doi.org/10.1186/s12934-024-02509-8.
[94] T. Schwanemann, N. Krink, P.I. Nikel, B. Wynands, N. Wierckx, Engineered passive glucose uptake in *Pseudomonas taiwanensis* VLB120 increases resource efficiency for bioproduction, Microb. Biotechnol. 18 (1) (2025) e70095, https://doi.org/10.1111/1751-7915.70095.
[95] S. Pauli, M. Kohlstedt, J. Lamber, F. Weiland, J. Becker, C. Wittmann, Systems metabolic engineering upgrades *Corynebacterium glutamicum* for selective high-level production of the chiral drug precursor and cell-protective extremolyte L-pipecolic acid, Metab. Eng. 77 (2023) 100–117, https://doi.org/10.1016/j.ymben.2023.03.006.
[96] S.L. Hoffmann, M. Kohlstedt, L. Jungmann, M. Hutter, I. Poblete-Castro, J. Becker, C. Wittmann, Cascaded valorization of brown seaweed to produce l-lysine and value-added products using *Corynebacterium glutamicum* streamlined by systems metabolic engineering, Metab. Eng. 67 (2021) 293–307, https://doi.org/10.1016/j.ymben.2021.07.010.
[97] S. Kind, S. Neubauer, J. Becker, M. Yamamoto, M. Völkert, G.V. Abendroth, O. Zelder, C. Wittmann, From zero to hero - production of bio-based nylon from renewable resources using engineered *Corynebacterium glutamicum*, Metab. Eng. 25 (2014) 113–123, https://doi.org/10.1016/j.ymben.2014.05.007.
[98] C.M. Rohles, L. Gläser, M. Kohlstedt, G. Giesselmann, S. Pearson, A. del Campo, J. Becker, C. Wittmann, A bio-based route to the carbon-5 chemical glutaric acid and to bionylon-6,5 using metabolically engineered *Corynebacterium glutamicum*, Green Chem. 20 (20) (2018) 4662–4674, https://doi.org/10.1039/c8gc01901k.
[99] C. Rohles, S. Pauli, G. Giesselmann, M. Kohlstedt, J. Becker, C. Wittmann, Systems metabolic engineering of *Corynebacterium glutamicum* eliminates all by-products for selective and high-yield production of the platform chemical 5-aminovalerate, Metab. Eng. 73 (2022) 168–181, https://doi.org/10.1016/j.ymben.2022.07.005.
[100] S. Jovanovic Gasovic, D. Dietrich, L. Gläser, P. Cao, M. Kohlstedt, C. Wittmann, Multi-omics view of recombinant *Yarrowia lipolytica*: enhanced ketogenic amino acid catabolism increases polyketide-synthase-driven docosahexaenoic production to high selectivity at the gram scale, Metab. Eng. 80 (2023) 45–65, https://doi.org/10.1016/j.ymben.2023.09.003.
[101] J. Becker, A. Lange, J. Fabarius, C. Wittmann, Top value platform chemicals: bio-based production of organic acids, Curr. Opin. Biotechnol. 36 (2015) 168–175, https://doi.org/10.1016/j.copbio.2015.08.022.
[102] D. Salvachúa, C.W. Johnson, C.A. Singer, H. Rohrer, D.J. Peterson, B.A. Black, A. Knapp, G.T. Beckham, Bioprocess development for muconic acid production from aromatic compounds and lignin, Green Chem. 20 (21) (2018) 5007–5019, https://doi.org/10.1039/C8GC02519C.
[103] A. Lange, J. Becker, D. Schulze, E. Cahoreau, J.C. Portais, S. Haefner, H. Schröder, J. Krawczyk, O. Zelder, C. Wittmann, Bio-based succinate from sucrose: high-resolution ^{13}c metabolic flux analysis and metabolic engineering of the rumen bacterium *Basfia succiniciproducens*, Metab. Eng. 44 (2017) 198–212, https://doi.org/10.1016/j.ymben.2017.10.003.
[104] J. Becker, C. Wittmann, From systems biology to metabolically engineered cells-an omics perspective on the development of industrial microbes, Curr. Opin. Microbiol. 45 (2018) 180–188, https://doi.org/10.1016/j.mib.2018.06.001.
[105] C. Ling, G.L. Peabody, D. Salvachúa, Y.M. Kim, C.M. Kneucker, C.H. Calvey, M. A. Monninger, N.M. Munoz, B.C. Poirier, K.J. Ramirez, P.C. St John, S. P. Woodworth, J.K. Magnuson, K.E. Burnum-Johnson, A.M. Guss, C.W. Johnson, G.T. Beckham, Muconic acid production from glucose and xylose in *Pseudomonas putida* via evolution and metabolic engineering, Nat. Commun. 13 (1) (2022) 4925, https://doi.org/10.1038/s41467-022-32296-y.
[106] W.J. Choi, E.Y. Lee, M.H. Cho, C.Y. Choi, Enhanced production of cis,cis-muconate in a cell-recycle bioreactor, J. Ferment. Bioeng. 84 (1) (1997) 70–76, https://doi.org/10.1016/S0922-338X(97)82789-4.
[107] C.R. Amendola, W.T. Cordell, C.M. Kneucker, C.J. Szostkiewicz, M.A. Ingraham, M. Monninger, R. Wilton, B.F. Pfleger, D. Salvachúa, C.W. Johnson, G. T. Beckham, Comparison of wild-type KT2440 and genome-reduced EM42 *Pseudomonas putida* strains for muconate production from aromatic compounds and glucose, Metab. Eng. 81 (2024) 88–99, https://doi.org/10.1016/j.ymben.2023.11.004.
[108] A.Z. Werner, R. Clare, T.D. Mand, I. Pardo, K.J. Ramirez, S.J. Haugen, F. Bratti, G. N. Dexter, J.R. Elmore, J.D. Huenemann, G.L.T. Peabody, C.W. Johnson, N. A. Rorrer, D. Salvachua, A.M. Guss, G.T. Beckham, Tandem chemical deconstruction and biological upcycling of poly(ethylene terephthalate) to beta-ketoadipic acid by *Pseudomonas putida* KT2440, Metab. Eng. 67 (2021) 250–261, https://doi.org/10.1016/j.ymben.2021.07.005.
[109] K.P. Sullivan, A.Z. Werner, K.J. Ramirez, L.D. Ellis, J.R. Bussard, B.A. Black, D. G. Brandner, F. Bratti, B.L. Buss, X. Dong, S.J. Haugen, M.A. Ingraham, M. O. Konev, W.E. Michener, J. Miscall, I. Pardo, S.P. Woodworth, A.M. Guss, Y. Román-Leshkov, S.S. Stahl, G.T. Beckham, Mixed plastics waste valorization through tandem chemical oxidation and biological funneling, Science 378 (6616) (2022) 207, https://doi.org/10.1126/science.abo4626.
[110] W.R. Henson, A.W. Meyers, L.N. Jayakody, A. DeCapite, B.A. Black, W. E. Michener, C.W. Johnson, G.T. Beckham, Biological upgrading of pyrolysis-derived wastewater: engineering *Pseudomonas putida* for alkylphenol, furfural, and acetone catabolism and (methyl)muconic acid production, Metab. Eng. 68 (2021) 14–25, https://doi.org/10.1016/j.ymben.2021.08.007.
[111] K.E. Nelson, C. Weinel, I.T. Paulsen, R.J. Dodson, H. Hilbert, V.A. Martins dos Santos, D.E. Fouts, S.R. Gill, M. Pop, M. Holmes, L. Brinkac, M. Beanan, R. T. DeBoy, S. Daugherty, J. Kolonay, R. Madupu, W. Nelson, O. White, J. Peterson, H. Khouri, I. Hance, P. Chris Lee, E. Holtzapple, D. Scanlan, K. Tran, A. Moazzez, T. Utterback, M. Rizzo, K. Lee, D. Kosack, D. Moestl, H. Wedler, J. Lauber, D. Stjepandic, J. Hoheisel, M. Straetz, S. Heim, C. Kiewitz, J.A. Eisen, K. N. Timmis, A. Dusterhoft, B. Tummler, C.M. Fraser, Complete genome sequence and comparative analysis of the metabolically versatile *Pseudomonas putida* KT2440, Environ. Microbiol. 4 (12) (2002) 799–808, https://doi.org/10.1046/j.1462-2920.2002.00366.x.
[112] B. Wunderlich, Thermal Analysis, 1 ed, Academic Press, 1990.
[113] D.R. Vardon, M.A. Franden, C.W. Johnson, E.M. Karp, M.T. Guarnieri, J.G. Linger, M.J. Salm, T.J. Strathmann, G.T. Beckham, Adipic acid production from lignin, Energy Environ. Sci. 8 (2) (2015) 617–628, https://doi.org/10.1039/C4ee03230f.
[114] B.J. Kim, W.J. Choi, E.Y. Lee, C.Y. Choi, Enhancement of *cis, cis*-muconate productivity by overexpression of catechol 1,2-dioxygenase in *Pseudomonas putida* BCM114, Biotechnol. Bioprocess Eng. 3 (2) (1998) 112–114, https://doi.org/10.1007/BF02932513.
[115] S.G. Bang, C.Y. Choi, DO-stat fed-batch production of *cis, cis*-muconic acid from benzoic acid by *Pseudomonas putida* BM014, J. Ferment. Bioeng. 79 (4) (1995) 381–383, https://doi.org/10.1016/0922-338X(95)94001-8.